THE GEOLOGICAL SOCIETY OF AMERICA®

Lithospheric architecture and tectonic evolution of the southwestern U.S. Cordillera: Constraints from zircon Hf and O isotopic data

J.B. Chapman[1,†], M.N. Dafov[1], G. Gehrels[1], M.N. Ducea[1,2], J.W. Valley[3], and A. Ishida[3,4]

[1]*Department of Geosciences, University of Arizona, Tucson, Arizona 85721, USA*

[2]*Faculty of Geology and Geophysics, University of Bucharest, 010041, Bucharest, Romania*

[3]*Wisconsin Secondary Ion Mass Spectrometer Laboratory, Department of Geoscience, University of Wisconsin, Madison, Wisconsin 53706, USA*

[4]*Institute for Excellence in Higher Education, Tohoku University, Sendai 9808576, Japan*

ABSTRACT

Radiogenic and stable isotopic studies of zircon are a powerful tool to investigate geologic processes because data can be placed in a temporal context using U-Pb ages. However, when zircon data lack information on the spatial distribution of the parent rock(s) (e.g., detrital data sets), interpreting changes in isotopic composition through time is not always straightforward. To evaluate and improve the utility of zircon isotopic data, we present a regional data set consisting of new zircon U-Pb, $\varepsilon Hf_{(t)}$, and $\delta^{18}O_{zrc}$ data in 31 Triassic to early Miocene igneous rocks from a >1300-km-long transect in the southwestern U.S. Cordillera. This data set is combined and compared with a compilation of whole rock isotopic data from the same transect. Orogen-scale spatial and temporal isotopic trends are identified and interpreted, both in terms of the underlying mechanisms that generated the trends and the tectonic processes that have shaped this part of the Cordillera. Most Cordilleran magmatism originates in the upper mantle and zircon $\varepsilon Hf_{(t)}$ primarily reflects the isotopic composition of the mantle source region. East of ~114°W longitude in the southwestern U.S. Cordillera, the continental mantle lithosphere remained coupled to the crust until the late Miocene and zircon $\varepsilon Hf_{(t)}$ reflects the age of the lithosphere. Because the mantle lithosphere remained intact, zircon $\varepsilon Hf_{(t)}$ and $\delta^{18}O_{zrc}$ of igneous rocks associated with low-angle to flat-slab subduction and crustal thickening during the Laramide orogeny are not significantly different from igneous rocks associated with Farallon slab rollback/foundering. Temporal isotopic trends identified in rocks east of ~114°W longitude are related to migration of magmatism into lithospheric terranes of a different age. West of ~114°E longitude, in regions like the Mojave Desert in southern California, USA, the continental mantle lithosphere is interpreted to have been partially removed and replaced by underplated Pelona–Orocopia–Rand schist and isotopically depleted asthenosphere or oceanic lithosphere during the Laramide orogeny. There is a temporal isotopic shift to more juvenile zircon $\varepsilon Hf_{(t)}$ and higher $\delta^{18}O_{zrc}$ in igneous rocks west of ~114°W, which is used to estimate the position of the western edge of intact North American continental mantle lithosphere before and after the Laramide orogeny. The results suggest that regional (spatial) trends in zircon $\varepsilon Hf_{(t)}$ and $\delta^{18}O_{zrc}$ data can be significantly larger than isotopic shifts at a specific location within a Cordilleran orogenic system. By accounting for regional spatial variations, temporal isotopic trends in zircon data can be more confidently interpreted in terms of tectonic and geodynamics processes.

1. INTRODUCTION

A defining characteristic of Cordilleran orogenic systems is a rich record of subduction-related magmatism, which provides insight into lithospheric architecture as well as tectonic and geodynamic processes (Ducea et al., 2015). Continental subduction systems and Cordilleran orogens cycle (10s m.y.) between extensional and contractional end-members, a fundamental feature in models for orogenic cyclicity (DeCelles et al., 2009; DeCelles and Graham, 2015; Ramos, 2009; Wells et al., 2012). The radiogenic isotopic composition of continental arc magmatism is a key tool used to track these cycles (Ducea, 2001; Haschke et al., 2002; Ducea and Barton, 2007). Kemp et al. (2009) demonstrated that zircon Lu-Hf and zircon O isotope ratios in igneous rocks can help distinguish contractional and extensional periods such as: slab roll-back, back-arc basin extension, basin closure, and lithospheric thickening. Zircon Lu-Hf isotopic data, including detrital zircon data, have recently been examined in numerous orogens to understand these processes and to help interpret periods of contraction and extension in the geologic record (Zhu et al., 2011; Boekhout et al., 2015; Balgord, 2017). However, a recent review of Cordilleran orogenic magmatism by Chapman et al. (2017) suggests that the isotopic composition of the continental lithosphere and, in particular, the presence or absence of the mantle lithosphere may exert a primary control on the zircon Lu-Hf isotopic composition of magmatic products. In this view, temporal shifts in the isotopic composition of magmatism in Cordilleran orogens are commonly related to the migration of magmatism into different lithospheric provinces or into regions with more or less continental mantle lithosphere preserved.

The southwestern U.S. Cordillera has experienced multiple episodes of extension, contraction, and arc migration during the Mesozoic to Cenozoic and the magmatic record is nearly continuous during this time (DeCelles, 2004; Dickinson, 2004; DeCelles and Graham, 2015). The impetus for this study was to test if the zircon Lu-Hf and zircon O isotopic composition of Mesozoic to early Miocene igneous rocks from the southwestern U.S. Cordillera reflect geodynamic changes. The results presented constitute the first regional zircon Lu-Hf and zircon O isotopic data set from Mesozoic and younger igneous rocks in this part of the U.S. Cordillera (Fig. 1; Table 1).

2. GEOLOGIC BACKGROUND: SOUTHWESTERN U.S. CORDILLERA

The U.S. Cordillera evolved since Paleozoic time as a result of subduction of oceanic lithosphere beneath the western North American

†jaychapman@email.arizona.edu

 https://doi.org/10.1130/B31937.1; 8 figures; 1 table; Data Repository item 2018202.

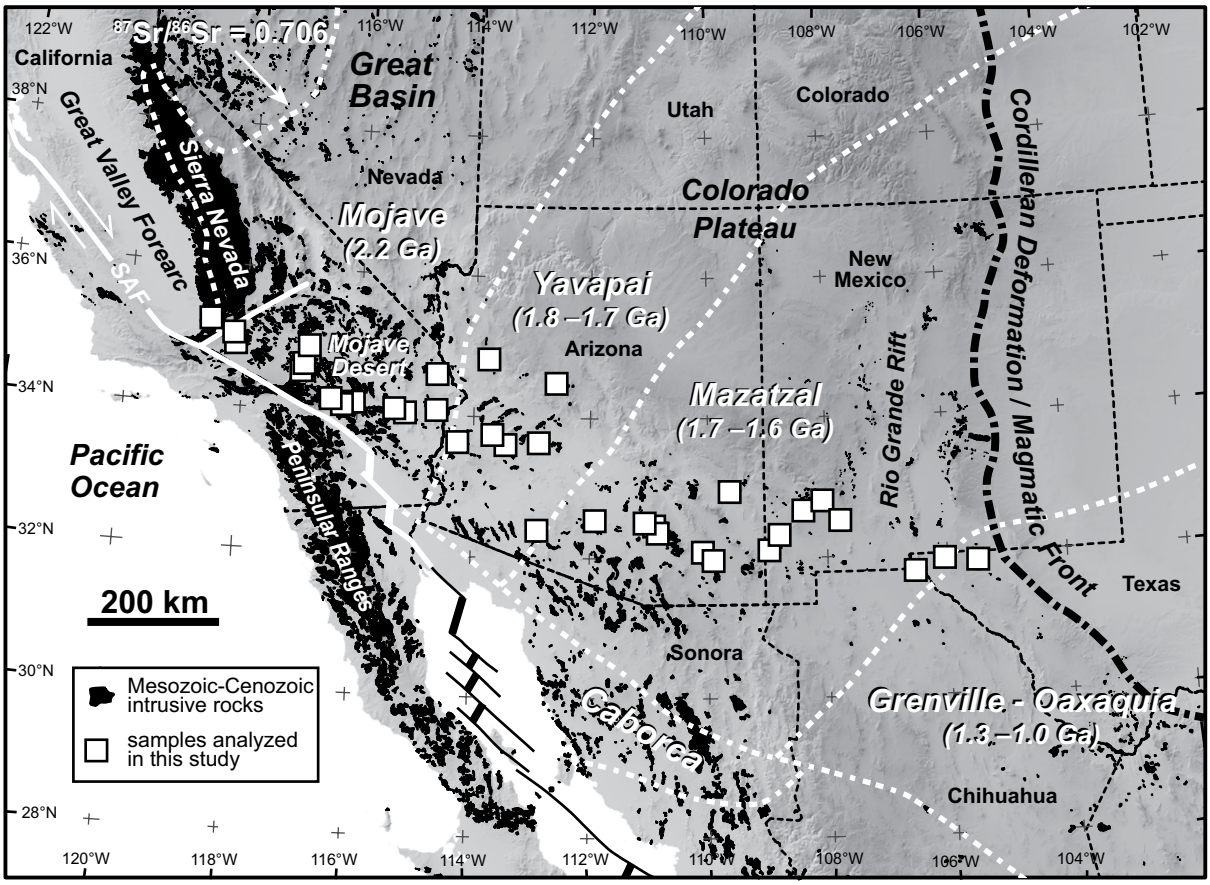

Figure 1. Regional map of the southwestern U.S. Cordillera showing the boundaries (white dashed lines) and Nd model ages (in parentheses) of major crustal provinces (Dickinson and Lawton, 2001b; Whitmeyer and Karlstrom, 2007; Wooden et al., 2013). $^{87}Sr/^{86}Sr = 0.706$ position from Kistler (1990). SAF—San Andreas fault. Sample location information is presented in Table 1.

plate (Dickinson, 2004). Widespread subduction beneath North America initiated during the Triassic and lasted until the subduction of the Pacific-Farallon mid-oceanic spreading center and development of the San Andreas transform plate boundary during the late Oligocene to Miocene (Atwater and Stock, 1998). Opening of the North Atlantic Ocean during the Middle Jurassic coincided with an increase in the North America–Farallon convergence rate and may have been linked to the start of contractional deformation in the Sevier retroarc thrust belt in the central U.S. Cordillera (DeCelles, 2004). In contrast to the central U.S. Cordillera, during the Jurassic, much of the southwestern U.S. Cordillera was marked by extension and the development of the Bisbee-Sabinas rift basin that has been linked to the opening of the Gulf of Mexico (Dickinson and Lawton, 2001a) and back-arc to intra-arc transtension (DeCelles, 2004; Busby, 2012). Subduction rollback of the Farallon plate facilitated this extension and led to rifting of the Guerrero terrane and opening of the Arperos Basin (Lawton and McMillan, 1999; Martini et al., 2014) (Fig. 2A). Regional extension and rifting might be expected to shift Lu-Hf isotope ratios in continental arc rocks to more juvenile compositions (cf., Boekhout et al., 2015). Rifting and post-extension thermal subsidence lasted until the mid-Cretaceous (ca. 100 Ma) at which time the Arperos Basin closed and the region transitioned into a contractional environment (Dickinson and Lawton, 2001a; Spencer et al., 2011; Martini et al., 2014). Despite widespread extensional deformation during the Jurassic, regionally significant shortening also occurred in the East Sierran thrust system (Dunne and Walker, 2004).

From the mid-Cretaceous to the start of the Laramide orogeny (ca. 80 Ma), foreland basin deposits (Barth et al., 2004; Spencer et al., 2011; Clinkscales and Lawton, 2015) and shortening in the Maria fold-thrust belt (Spencer and Reynolds, 1990) and Mexican fold-thrust belt (Fitz-Díaz et al., 2017) suggest that the southwestern U.S. Cordillera was part of a retroarc thrust belt and retroarc foreland basin system (Fig. 2B). Prior to the Laramide orogeny, oceanic subduction is recorded by calc-alkaline, intermediate (andesitic), sublinear volcanic arcs and batholiths (Dickinson, 2004). The southwestern U.S. Cordilleran subduction system initiated during the Late Permian (Walker, 1988) and produced voluminous (high-flux) magmatic events during the (1) Triassic (Riggs et al., 2013); (2) the Late Jurassic (Barth et al., 2017); and (3) the mid- to Late-Cretaceous that comprises the bulk of the Sierra Nevada and Peninsular Ranges batholiths (Cecil et al., 2012).

The Laramide orogeny (80–40 Ma) is thought to be related to low-angle or flat-slab subduction of the Farallon plate (Fig. 2C), associated with subduction of an oceanic plateau (Coney and Reynolds, 1977; Saleeby, 2003; Liu et al., 2010). Continental arc magmatism in the Sierra Nevada and Peninsular Ranges batholiths ended by ca. 80 Ma (Ducea, 2001) and magmatism migrated eastward toward the foreland, reaching its maximum eastern extent in the Big Bend region of Texas, USA, and Sierra Madre Oriental in Mexico during the Late Eocene (Constenius et al., 2003; Fitz-

TABLE 1. SAMPLE INFORMATION AND DATA SUMMARY

Sample	Latitude (°N)	Longitude (°E)	U-Pb age (Ma)	$\varepsilon Hf_{(t)}$	$\delta^{18}O_{zrc}$ (‰)	Rock type	Pluton name
Neogene							
Barstow_T	34.8960	−116.8960	18.2 ± 0.7	−5.0 ± 2.8		Andesite	N/A
Buckeye	33.6200	−112.8800	20.0 ± 0.7	−3.9 ± 0.7		Granite	Belmont
Reefer	35.0070	−118.1720	20.3 ± 0.8	4.5 ± 1.2	8.4 ± 0.2	Rhyolite	N/A
Snaggletooth	34.5830	−114.6420	20.3 ± 0.9	−5.8 ± 2.2	6.4 ± 0.3	Dacite	N/A
Paleogene							
Cochise	31.9441	−109.9570	26.1 ± 1.8	−7.1 ± 1.4	6.2 ± 0.5	Quartz monzonite	Cochise Stronghold
Granite_Gap	32.0907	−108.9723	34.2 ± 1.2	−9.3 ± 1.8	5.2 ± 0.8	Quartz monzonite	Granite Gap
Hueco	31.9210	−106.0480	34.9 ± 1.2	−1.4 ± 2.2	4.8 ± 0.3	Quartz syenite	Hueco Tanks
Tinaja	31.8610	−105.4778	35.7 ± 1.1	−0.5 ± 3.8	5.3 ± 0.4	Nepheline syenite	Miller Mountain
Cooke	32.5000	−107.7730	39.4 ± 1.5	−7.8 ± 1.9	5.1 ± 1.2	Granodiorite	Cookes Peak
UTEP	31.7838	−106.5082	46.7 ± 2.2	−3.9 ± 2.1		Monzodiorite	Campus Andesite
Tyrone	32.6513	−108.3658	56*	−5.5 ± 1.7		Quartz monzonite	Tyrone
Dragoon	32.0572	−110.0832	55.5 ± 1.9	−12.1 ± 2.5	6.6 ± 1.6	Quartz monzonite	Texas Canyon
San Juan	32.9456	−109.6517	59*	−3.4 ± 1.2		Quartz monzonite	San Juan
Chino	32.7954	−108.0632	60*	−4.0 ± 1.1		Granodiorite	Santa Rita
Ajo	32.3551	−112.8656	63*	−8.6 ± 0.8		Granodiorite	Cornelia
Cretaceous							
Lakeshore	32.5226	−111.9048	70*	−9.9 ± 1.6		Granodiorite	Lakeshore
Granite_Mtn	34.0330	−115.2290	71.5 ± 2.8	−12.3 ± 1.0	6.2 ± 0.2	Granodiorite	Granite Pass
Hope	33.7350	−113.6700	72.7 ± 2.3	−11.1 ± 1.8	5.6 ± 0.3	Granodiorite	Granite Wash
JDP	34.8242	−113.7378	72.8 ± 3.2	−13.5 ± 1.5		Quartz monzonite	Diamond Joe
Coxcomb	34.0800	−115.3620	76.1 ± 3.4	−11.0 ± 2.0	6.9 ± 1.1	Granodiorite	Coxcomb
Yucca	34.1430	−116.4150	76.9 ± 3.1	−8.3 ± 2.1	7.0 ± 1.2	Quartz monzonite	Cactus
Joshua	34.1230	−116.3000	77.0 ± 5.2	−13.8 ± 6.3	6.2 ± 1.2	Monzogranite	Panorama
Prescott	34.4928	−112.5781	80.2 ± 6.7	−9.3 ± 0.9		Quartz monzonite	Copper Basin
Rosamond	34.8890	−118.1510	88.4 ± 2.6	−4.9 ± 2.0		Quartz monzonite	Rosamond Hills
Riverside	34.0860	−114.6640	100.8 ± 3.6	−6.1 ± 3.6	5.4 ± 0.5	Quartz monzodiorite	W. Riverside Mtn.
Keene	35.2200	−118.5600	102.7 ± 3.5	5.8 ± 2.1	7.0 ± 0.6	Tonalite	Bear Valley
Jurassic							
Strawberry	34.5550	−117.0000	148.8 ± 4.7	−9.6 ± 1.7	5.3 ± 0.9	Granodiorite	unknown
S_Barstow	34.6390	−116.9480	161.2 ± 4.6	−6.0 ± 2.3	5.4 ± 0.6	Quartz monzonite	unknown
Quartzite	33.6490	−114.2610	165.0 ± 4.2	−10.4 ± 1.3	5.2 ± 0.5	Quartz monzonite	Julian Mine
Finger	33.6010	−113.4600	171.0 ± 5.0	−9.5 ± 1.5		Granodiorite	Lone Mountain
Triassic							
29-Palms	34.1260	−116.1130	234†		5.2 ± 0.4	Quartz monzonite	Twentynine Palms

Note: UTEP—University of Texas at El Paso; JDP—Diamond Joe Peak.
*From Leveille and Stegen (2012).
†From Barth and Wooden (2006).

Díaz et al., 2017). Most Laramide-age magmatism is calc-alkaline, metaluminous, and associated with subduction processes (Lang and Titley, 1998; McMillan, 2004). A broad belt of Laramide-age peraluminous (S-type) granite is also present in the Cordillera and has been attributed to crustal anatexis (Miller and Barton, 1990). Crustal melting may have been driven by asthenospheric upwelling following delamination (Wells et al., 2012) or by radiogenic heating associated with crustal thickening (Farmer and DePaolo, 1984). The Laramide orogeny in the southwestern U.S. Cordillera is associated with basement-involved, high-angle reverse faulting, block uplifts, and localized basin sedimentation associated with these uplifts (Davis, 1979; Dickinson et al., 1988; Clinkscales and Lawton, 2015) (Fig. 2C). Crustal thickening and contraction associated with the Laramide orogeny might be expected to shift Lu-Hf isotope ratios in magmatic rocks to more evolved compositions (cf., Boekhout et al., 2015). Isolated exposures of the Late Cretaceous to Eocene Pelona–Orocopia–Rand schist are present in the southwestern U.S. Cordillera west of ~113.5°W longitude and are inferred to be the result of subduction erosion and underplating of the accretionary complex and forearc during the Laramide orogeny (Grove et al., 2003; Ducea et al., 2009; Chapman, 2017 and references therein).

The end of the Laramide orogeny in the southwestern U.S. Cordillera is marked by a transition from contractional to extensional tectonics around 40 Ma (Constenius et al., 2003) (Fig. 3). The transition to extension is generally attributed to rollback and foundering of the Farallon slab, which has also been associated with a rapid westward sweep of magmatism toward the plate margin (Fig. 2D) (Coney and Reynolds, 1977; Humphreys, 1995). This magmatic event lasted in the Cordilleran interior until the middle Miocene, was widespread, voluminous, and includes the "ignimbrite flare-up" of western North America with a peak in activity between 25 and 30 Ma (Lipman, 1992). During the Oligocene to early Miocene, extension initiated in the Rio Grande rift (Ricketts et al., 2016) and large-magnitude slip on low-angle normal fault systems helped to exhume a series of metamorphic core complexes in the Colorado River extensional corridor, southern Arizona, Sonora, and the eastern Mojave region (Dickinson, 1991) (Fig. 2D). Dickinson (1991) referred to this stage (ca. 30–15 Ma) of extension, dominated by low-angle normal faulting, as the mid-Tertiary taphrogeny and distinguished it from subsequent "Basin and Range" extension within the southwestern U.S. Cordillera. Lithospheric extension and extension during this time might be expected to shift Lu-Hf isotope ratios in magmatic rocks to more juvenile compositions (cf., Boekhout et al., 2015).

Basin and Range style extension is most prominent in the central part of southwestern U.S. Cordillera (Arizona, New Mexico) and is characterized by high-angle normal faults and the formation of ~north-south–trending half-graben systems (Dickinson, 1991; Spencer et al., 1995). The majority of Basin and Range style extension occurred between the middle Miocene and Pliocene (McQuarrie and Wernicke, 2005). Starting in the Miocene, there was a pronounced shift in the composition of magmatism in the U.S. Cordillera. Intermedi-

ate to felsic ignimbrite-related magmatism was replaced by bimodal, predominantly basaltic, magmatism (Armstrong and Ward, 1991). This shift is closely linked to Basin and Range extension and as extension progressed from the late Miocene to the present, magmatism in the southwestern U.S. Cordillera became increasingly characterized by the eruption of tholeiitic and alkali basalt with asthenospheric major and trace element patterns and juvenile isotopic compositions (e.g., Wang et al., 2002). The start of Basin and Range extension is interpreted to mark the end of the Cordilleran-style orogenic processes and magmatism <15 Ma is not considered in this study.

2.1. Lower Crustal Structure and Basement Terranes, Southwestern U.S. Cordillera

The central U.S. Cordillera contains terranes of possible allochthonous origin (e.g., Roberts Mountains allochthon) that were accreted to the North American plate in the Paleozoic (e.g., Antler orogeny; Speed and Sleep, 1982; Dickinson, 2004). Several isotopic studies on magmatic rocks have helped to delineate the boundary between these terranes and North American basement rocks (King et al., 2004 and references therein); however, the boundary is most commonly associated with the $^{87}Sr/^{86}Sr$ = 0.706 isopleth, colloquially called the "706 line" (Kistler and Peterman, 1973) (Fig. 1). More radiogenic (evolved) isotopic values in Mesozoic and Cenozoic igneous rocks occur east of the 706 line. In the southwestern U.S. Cordillera, the 706 line parallels the crest of the southern Sierra Nevada and is truncated against the Garlock fault (Kistler, 1990) (Fig. 1). The 706 line in the southern Sierra Nevada has been interpreted to mark the edge of continental basement (Kistler, 1990) as well as the edge of North American mantle lithosphere (Coleman and Glazner, 1997). Mantle xenoliths from the eastern Sierra Nevada indicate that the base of the mantle lithosphere was located at >100 km depth during the Mesozoic and that the radiogenic isotopic compositions of Mesozoic plutons in the eastern Sierra Nevada are similar to the isotopic composition of the Mesozoic mantle lithosphere (Ducea and Saleeby, 1998; Ducea, 2001).

The southwestern U.S. Cordillera does not contain any large accreted terranes like the central and northern U.S. Cordillera. There are a few ranges in the northwest Mojave Desert region (e.g., El Paso Mountains) containing basement rocks correlated with the Roberts Mountains allochthon that have been displaced southward by sinistral strike slip and then thrust over North American lithosphere (Miller et al., 1995), but samples from this study did not come from these locations. North American crystalline basement is thought to extend westward across the Mojave region to the San Andreas fault (Martin and Walker, 1992) and the thickest section of the North American Proterozoic to Paleozoic passive margin sequence (Cordilleran miogeocline) occurs in the western Mojave region (Stewart, 2005).

The Proterozoic continental lithosphere in the southwestern U.S. Cordillera consists of several tectonostratigraphic terranes or provinces including, from oldest to youngest, the Mojave, Yavapai, Mazatzal, and Grenville terranes (Whitmeyer and Karlstrom, 2007) (Fig. 1). The Mojave crustal province records Paleoproterozoic continental crust formation, incorporates rocks as old as the Archean, and has a mean crustal Sm-Nd model age of ca. 2.2 Ga (Wooden et al., 2013). Formation and accretion of juvenile crust occurred in the Yavapai province at 1.7–1.8 Ga, the Mazatzal province at 1.6–1.7 Ga, and the Grenville province at 1.0–1.3 Ga (Whitmeyer and Karlstrom, 2007 and references therein). The Nd isotopic composition of Mesozoic and younger magmatic rocks has been used to define isotopic provinces, which roughly mimic the geographic position of Proterozoic terranes based on U-Pb studies (Bennett and DePaolo, 1987).

Figure 2 (*on following page*). Schematic tectonic maps and interpretive cross-sections of the southwestern U.S. Cordillera from the Late Jurassic to mid-Miocene. The heavy gray dashed line in maps and in cross-sections denotes the inferred edge of intact North American continental mantle lithosphere. Cross-sections are vertically aligned using the approximate reconstructed position of the Arizona–New Mexico border (~109°E longitude). (A) 150–100 Ma, subduction roll-back of the Farallon plate contributed to an extensional tectonic regime and opening of the Bisbee rift basin (Dickinson and Lawton, 2001a). The continental mantle lithosphere was the mantle source for Jurassic magmatism in western California and southern Arizona. (B) 100–80 Ma, closure of the Arperos Basin and suturing of the Guerrero terrane (Martini et al., 2014) led to the development of a contractional tectonic regime including a retroarc thrust belt and foreland basin (Clinkscales and Lawton, 2015; Fitz-Díaz et al., 2017). The Sierra Nevada and Peninsular Ranges batholiths formed above the transition between asthenospheric upper mantle and continental mantle lithosphere (Coleman and Glazner, 1997). (C) 80–40 Ma, the Laramide orogeny is associated with low-angle to flat-slab subduction, subduction erosion of the accretionary complex and forearc, underplating of the Pelona–Orocopia–Rand (POR) schist, arc migration toward the foreland, and increased contraction forming block uplifts and localized sedimentary basins (Coney and Reynolds, 1977; Dickinson et al., 1988; Saleeby, 2003; Chapman, 2017). Most Laramide-age magmatism is interpreted to have originated in the continental mantle lithosphere. By the end of the Laramide, the continental mantle lithosphere in the Mojave region (west of ~114°W longitude) had been at least partially removed. (D) 40–15 Ma, foundering or roll-back of the Farallon slab and subduction of the Pacific-Farallon spreading center resulted in an extensional tectonic regime, metamorphic core-complex formation (Dickinson, 1991) and a rapid westward sweep of ignimbrite magmatism (Humphreys, 1995). The mantle source of magmatism west of ~114°W longitude was the depleted asthenospheric mantle or Farallon oceanic lithosphere (Miller et al., 2000) and the mantle source east of ~114°W longitude was the continental mantle lithosphere (Farmer et al., 2008).

3. ANALYTICAL METHODS

Rock samples were processed at the University of Arizona using standard methods for isolating zircon, including magnetic and heavy liquid separation techniques. Zircon crystals from the same sample were used for U-Pb geochronology, Lu-Hf isotope geochemistry, and O isotope geochemistry. Zircon crystals were mounted in epoxy along with relevant standards and then polished to expose a cross-section of the crystal interior. Epoxy mounts were imaged by backscatter electron (BSE) and cathodoluminescence (CL) detectors on a Hitachi 3400N scanning electron microscope (SEM) at the Arizona LaserChron SEM facility. Locations for zircon U-Pb, Lu-Hf, and O isotopic analyses were chosen using a combination of high-resolution BSE and CL images.

U-Th-Pb isotope ratios were collected at the University of Arizona LaserChron Center (www.laserchron.org) using a Teledyne Photon Machines G2™ solid state NeF excimer laser ablation system coupled to a Thermo Fisher Scientific ELEMENT 2™ single collector inductively coupled plasma–mass spectrometer (SC-ICP-MS). Data were collected and reduced following the procedures described by Gehrels et al. (2008) and Gehrels and Pecha (2014). The value, uncertainty, and scatter of the zircon stan-

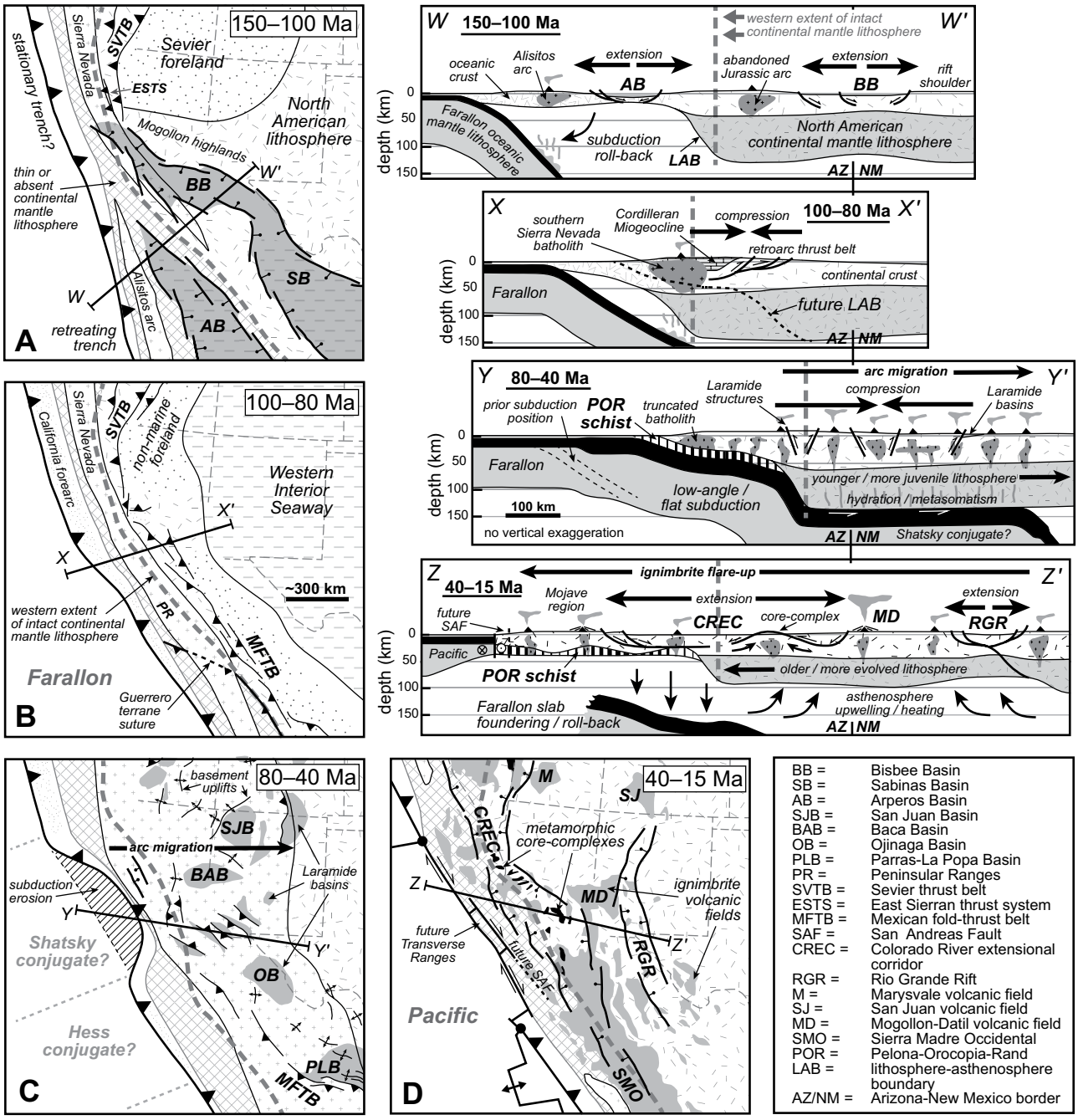

Figure 2.

dards during the analytical sessions was 1098.7 ± 0.7 Ma for the primary standard FC-1 (range = 1004–1199 Ma), 557.0 ± 0.4 Ma for the secondary standard SL (range = 532–587 Ma), and 418.2 ± 0.4 Ma for the secondary standard R33 (range = 399–439 Ma). All analyses with acceptable precision, discordance, and in-run fractionation are presented in Table DR1 in the Data Repository.[1] Acceptable discordance (comparing $^{206}Pb/^{238}U$ and $^{206}Pb/^{207}Pb$ ages) is <20% and <5% for reverse discordance. Discordance filters are only applied to ages >400 Ma. The reported U-Pb age for each sample is a weighted mean of 5–23 individual zircon U-Pb analyses. Because all samples have Mesozoic or younger crystallization ages, $^{206}Pb/^{238}U$ ratios were used to calculate weighted mean ages. Uncertainty is reported at the 2σ level and includes internal and external uncertainties added in quadrature (Table 1).

Zircon Lu-Hf isotope geochemistry was conducted by LA-ICP-MS at the Arizona LaserChron Center using a Nu Instruments multicollector mass spectrometer coupled to a Teledyne Photon Machines G2™ laser system. Measurements were made using a 40 µm diameter spot placed directly over a previous 20 µm U-Pb ablation pit. Data collection and reduction follows the procedures described in Cecil et al. (2011) and Gehrels and Pecha (2014). After adjusting

[1]GSA Data Repository item 2018202, Supplementary File 1 and Tables DR1–DR4, is available at http://www.geosociety.org/datarepository/2018 or by request to editing@geosociety.org.

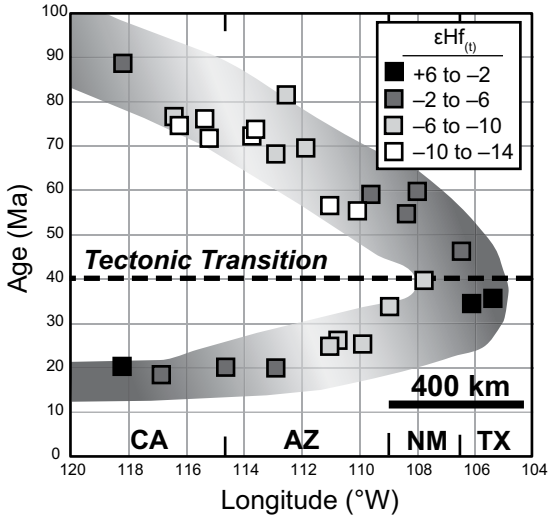

Figure 3. Plot of age versus longitude for igneous rocks in the southern U.S. Cordillera showing the eastward (100–40 Ma) and then westward (40–15 Ma) migration of magmatism (Table 1). A previous compilation of igneous rock age data (shaded band) and estimate of the tectonic transition from a contractional to extensional regime is adopted from Constenius et al. (2003). CA—California; AZ—Arizona; NM—New Mexico; TX—Texas. Squares are samples analyzed in this study and shaded by mean zircon $\varepsilon Hf_{(t)}$ (Table 1).

mass bias to reduce offset, the value, uncertainty, and scatter of the zircon standards during the analytical sessions was 0.28218 ± 0.00005 $^{176}Hf/^{177}Hf$ for FC-52 (range = 0.28208–0.28269 $^{176}Hf/^{177}Hf$), 0.28267 ± 0.00003 $^{176}Hf/^{177}Hf$ for Temora-2 (range = 0.28259–0.28274 $^{176}Hf/^{177}Hf$), 0.28254 ± 0.00003 $^{176}Hf/^{177}Hf$ for Mud Tank (range = 0.28247–0.28259 $^{176}Hf/^{177}Hf$), 0.28250 ± 0.00004 $^{176}Hf/^{177}Hf$ for Plesovice (range = 0.28245–0.28277 $^{176}Hf/^{177}Hf$), 0.28275 ± 0.00003 $^{176}Hf/^{177}Hf$ for R33 (range = 0.28266–0.28288 $^{176}Hf/^{177}Hf$), and 0.28232 ± 0.00005 $^{176}Hf/^{177}Hf$ for 91500 (range = 0.28219–0.28275 $^{176}Hf/^{177}Hf$). Lu-Hf isotopic data are presented throughout the paper using epsilon notation, in which $^{176}Hf/^{177}Hf$ ratios are expressed relative to the chondritic uniform reservoir (CHUR; Bouvier et al., 2008). $\varepsilon Hf_{(t)}$ refers to the εHf isotopic composition at the time of zircon crystallization. Results and internal precision for $^{176}Hf/^{177}Hf$ and εHf are reported for each analysis in Table DR2 (see footnote 1). Reported $\varepsilon Hf_{(t)}$ values are weighted means of 5–15 individual zircon $\varepsilon Hf_{(t)}$ analyses and 2σ uncertainties are reported by combining external and internal uncertainty in quadrature. Single zircon $\varepsilon Hf_{(t)}$ analysis values were excluded from mean sample values when the corresponding single-grain zircon U-Pb analysis indicated the spot was part of an inherited age domain (generally >3σ larger than the youngest age population; Table DR2).

Zircon oxygen isotope ratios were measured by secondary ion mass spectroscopy (SIMS) at the Wisconsin Secondary Ion Mass Spectrometer (WiscSIMS) laboratory at the University of Wisconsin–Madison using a CAMECA IMS 1280 ion microprobe using procedures described elsewhere (Kita et al., 2009; Valley and Kita, 2009 and references therein). Sample zircon grains were mounted in epoxy resin with the running reference material, KIM-5 zircon (Valley, 2003), and coated by gold. The primary Cs+ beam with intensity of ~1.6 nA, was focused to an analysis spot size of ~12 μm on a polished zircon surface (separate mounts from U-Pb Lu-Hf analyses). CL images of zircons from samples previously analyzed for U-Pb isotopes were used to guide analysis locations, although inadvertent analyses of multiple zircon age domains may have occurred. Secondary ions of $^{16}O^-$ and $^{18}O^-$ were detected by two Faraday Cup detectors for oxygen isotope analysis and $^{16}OH^-$ was detected by Faraday cup to monitor the influence of contaminant, simultaneously. For zircons, elevated OH/O ratios, when corrected for background, are typical for domains with high degree of radiation damage (Wang et al., 2014). A single analysis took 3 min, which includes an initial pre-sputtering (10s), automatic centering of secondary ions (~60s), and integration of oxygen isotope signals (4s × 20 cycle). Oxygen isotopic data is reported in per mil (‰) using delta notation relative to Vienna standard mean ocean water (VSMOW). Instrumental mass bias of oxygen isotope ratio was calibrated by bracketing analysis of KIM-5 zircon for every ~10 unknown analyses, typically four analyses at the start of each bracket and four at the end. Based on in-run analysis of KIM-5 zircon, the average precision of $\delta^{18}O_{zrc}$ is ≤0.3‰ (2 standard deviation [SD]). Reported $\delta^{18}O_{zrc}$ in Table 1 is a weighted mean of 7–13 individual zircon $\delta^{18}O$ analyses using 2 SD external precision as the weighting factor. The uncertainty of $\delta^{18}O_{zrc}$ values reported in Table 1 represents intra-sample variation and is reported as two standard deviations of the range of values from each sample. Complete results for unknown and standard analyses are presented in Data Repository DR3 (see footnote 1).

In addition to new analyses, existing εNd and $\delta^{18}O$ data were compiled from the North American Volcanic and Intrusive Rock Database (NAVDAT; navdat.org). The compiled data comes from the same geographic range as the transect samples and excludes samples <15 Ma, which are often characterized by juvenile isotopic compositions related to Basin and Range extension. A table of all compiled data and data sources is presented in Table DR4 (see footnote 1). Compiled $\delta^{18}O$ data comes from intrusive and extrusive whole rock samples and mineral analyses other than zircon. For comparison purposes, equilibrium fractionation ($\Delta^{18}O$) between whole rock and zircon analyses is estimated using the calibration from Lackey et al. (2008) that incorporates whole rock SiO_2 contents. Equilibrium fractionation at magmatic temperatures for other mineral-zircon pairs used to compare data in this study are; $\Delta^{18}O_{quartz\text{-}zrc}$ = 2.2; $\Delta^{18}O_{sanidine\text{-}zrc}$ = 1.45; $\Delta^{18}O_{plagioclase\text{-}zrc}$ = 1.0 (Bindeman and Valley, 2001; Valley et al., 2003; Trail et al., 2009). For comparison purposes, whole rock $\varepsilon Nd_{(t)}$ is related to zircon $\varepsilon Hf_{(t)}$ using the terrestrial array of Vervoort et al. (1999) and Beard and Johnson (1997). There is minor isotopic fractionation between zircon Hf analyses and the parent whole rock Hf analyses (Kinny and Maas, 2003), which allows the comparison of whole rock $\varepsilon Nd_{(t)}$ to zircon $\varepsilon Hf_{(t)}$. Converted εNd and $\delta^{18}O$ data are included in Table DR4.

4. RESULTS

Zircon was analyzed from 31 samples of igneous rocks (mainly intrusive) collected from an ~1300-km-long transect across the southwestern U.S. Cordillera, from the southern Sierra Nevada in California to West Texas (~118.5°W to ~105.5°W longitude and ~31.75°N to ~35.25°N latitude) (Fig. 1; Table 1). This study reports new zircon U-Pb ages for 25 samples, 30 new zircon Lu-Hf isotopic ranges, and 20 new zircon oxygen isotopic ranges (Table 1). Basic descriptions of each sample and detailed zircon U-Pb, zircon Lu-Hf, and zircon $\delta^{18}O$ results for each sample are provided in the Data Repository (see footnote 1). Samples were chosen based on geographic distribution (from a range of longitudes) and age (Mesozoic to early Miocene) to explore temporal and spatial isotopic changes (Figs. 2–4). Samples <15 Ma were avoided, as many igneous rocks of this age in the southwestern U.S. are associated with Basin and Range extension and their isotopic composition may not reflect Cordilleran (continental arc) tectonic processes. Igneous rock classification in Table 1 is based on appearance in the field or, when available, from chemical analyses published in previous studies (Supplemental File 1). Indi-

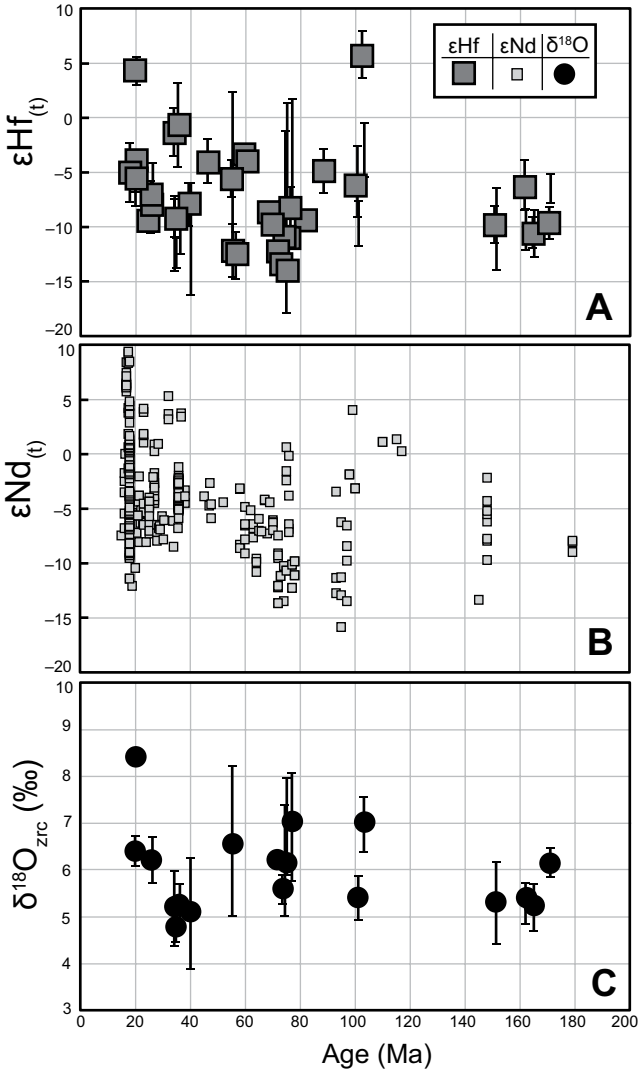

Figure 4. Plot of mean zircon U-Pb age versus (A) mean zircon $\varepsilon Hf_{(t)}$, (B) compiled age and whole rock $\varepsilon Nd_{(t)}$ of samples from the southern U.S. Cordillera, and (C) mean $\delta^{18}O_{zrc}$ for samples analyzed in this study (Table 1). εNd data are converted to equivalent εHf values using the terrestrial array (εHf = 1.36εNd + 2.95) of Vervoort et al. (1999). There is a possible increase in zircon $\varepsilon Hf_{(t)}$ from 100 to 20 Ma, however, temporal isotopic trends are not clearly present. Compiled data are available in Table DR4 (see footnote 1). Error bars for $\delta^{18}O_{zrc}$ data in panel C are sometimes smaller than the symbol.

vidual samples were not analyzed chemically in this study and are not intended to be representative of the entire compositional range of a pluton or intrusive suite.

4.1. Zircon U-Pb Geochronology Results

Results of zircon U-Pb geochronology are presented in Table 1. To our knowledge, all the ages presented are broadly consistent with previous studies. References to previous studies for individual plutons or igneous suites are provided for each sample in the Data Repository. All weighted mean zircon U-Pb ages presented in Table 1 are interpreted as crystallization/emplacement ages and exclude old ages obtained from premagmatic zircon cores and occasionally young ages interpreted to be related to loss of radiogenic Pb (Table DR1 and text). Average U/Th of zircon analyses used to calculate crystallization ages are <5 for all samples (Table DR1). Five of the samples (Tyrone, San Juan, Chino, Ajo, and Lakeshore) were previously dated by Leveille and Stegen (2012) using zircon U-Pb isotope geochronology. The age of sample 29-Palms was adopted from zircon U-Pb isotopic data presented in Barth and Wooden (2006). Late Cretaceous and younger igneous rocks in this study show the same spatial-temporal patterns (eastward migration followed by westward migration; Fig. 3) documented in previous compilations of igneous rock ages from the U.S. Cordillera (Coney and Reynolds, 1977; Constenius et al., 2003).

Pre-magmatic and/or xenocrystic cores were analyzed for U-Pb when encountered (based on CL images), but not investigated systematically. Premagmatic (inherited) zircon cores range in age from Mesozoic to Proterozoic (Supplemental Table DR1). Inherited (single-grain) ages are shown in Figure 5 where analyses are grouped by the crustal province the parent sample was collected from (Fig. 1). Although it is not a comprehensive data set, the Proterozoic inherited zircon ages are broadly consistent with published ranges of basement ages for the crustal provinces (Whitmeyer and Karlstrom, 2007), excluding inherited zircon ages from the Mojave province (sample size n = 11) and Yavapai province (n = 3), which are younger than expected.

4.2. Zircon Lu-Hf Isotope Results

Results of zircon Lu-Hf isotopic analyses are presented in Table 1, Figures 3–6, and Table DR2. Reported weighted mean zircon $\varepsilon Hf_{(t)}$ values are calculated from zircon grains that have U-Pb ages consistent with the crystallization/emplacement age. Most samples have uncertainties of <2 εHf units for mean values (Table 1), although uncertainty is high (up to 6 εHf units) for some samples.

Zircon $\varepsilon Hf_{(t)}$ data show little or no secular trend but significant regional distinctions. Plotting isotopic data from the southwestern U.S. Cordillera against sample age, as is commonly done for detrital zircon $\varepsilon Hf_{(t)}$ data (e.g., Gehrels and Pecha, 2014), revealed a possible trend of increasing $\varepsilon Hf_{(t)}$ from the Late Cretaceous to the early Miocene (Fig. 4A), although no clear trends are easily recognizable. A compilation of $\varepsilon Nd_{(t)}$ data from the southern U.S. Cordillera (Table DR4) also shows a large range of isotopic values at many points in time without a clear temporal trend (Fig. 4B).

Regional isotopic trends are most apparent when plotted against longitude (Fig. 6), which is sub-parallel to the structural grain of the Cordillera. Zircon $\varepsilon Hf_{(t)}$ data in Figure 6A form a broad U-shaped pattern with the most isotopically juvenile values (+10 to +15 $\varepsilon Hf_{(t)}$) in the western Mojave Desert and Sierra Nevada,

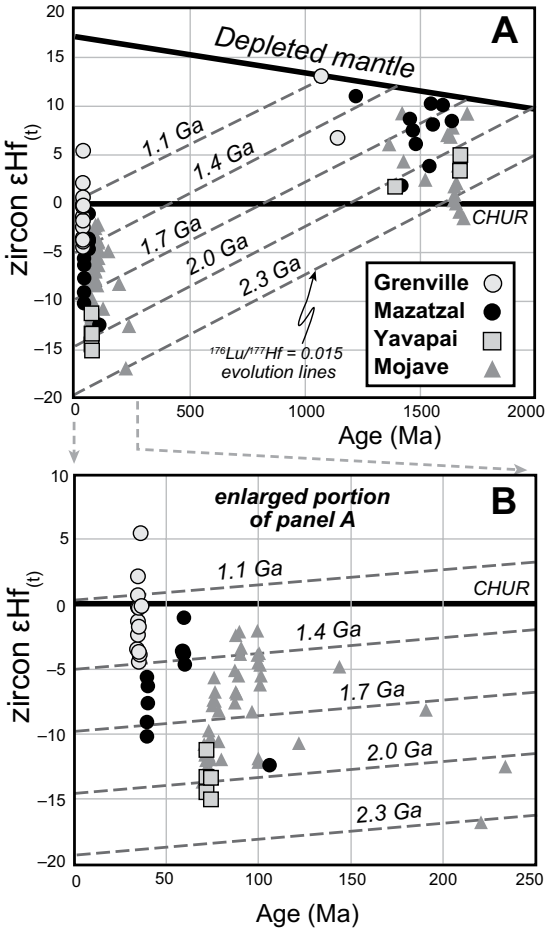

Figure 5. (A) Plot of individual (single-grain) zircon U-Pb age versus zircon $\varepsilon Hf_{(t)}$ for samples that contained inherited ages (e.g., premagmatic cores). Analyses are grouped by the lithospheric province they were sampled from (Fig. 1). Mesozoic-Cenozoic and Proterozoic analyses from the same province that plot along the same mean crustal evolution line suggest that the Mesozoic-Cenozoic igneous rocks were derived from a lithospheric source with a similar age and composition to the lithospheric province hosting the sample. Several analyses from the Mojave province do not fall along a common crustal evolution line. (B) An enlarged portion of panel A showing Mesozoic to Cenozoic analyses. CHUR—chondritic uniform reservoir. Zircon $\varepsilon Hf_{(t)}$ data are available in Table DR2 (see footnote 1).

the most isotopically evolved values (–10 to –15 $\varepsilon Hf_{(t)}$) around ~114°W longitude, and relatively juvenile values (0 to +10 $\varepsilon Hf_{(t)}$) in West Texas. The spatial change (ε/distance) in isotopic values is greatest (steepest) in the west. Compiled $\varepsilon Nd_{(t)}$ data in Figure 6A corroborate this trend.

Data in Figure 6A are separated into samples older and younger than 40 Ma, the approximate end of the Laramide orogeny and the initial age of a switch from a contractional to extensional tectonic regime in the southwestern U.S. Cordillera (Fig. 3; Constenius et al., 2003). The ">40 Ma" and "<40 Ma" bands in Figure 6A encompass all of the new Hf isotopic data and ~90% of the compiled Nd isotopic data. At any longitudinal position in the southwestern U.S. Cordillera there is variation in the isotopic composition of magmatic rocks, but most of these values fall within a ~10 epsilon unit range, outlined by dashed lines or "bands" in Figure 6A. In samples older than 40 Ma, the lowest $\varepsilon Hf_{(t)}$ and $\varepsilon Nd_{(t)}$ values occur at 117°W to 116°W longitude. Both $\varepsilon Hf_{(t)}$ and $\varepsilon Nd_{(t)}$ samples younger than 40 Ma exhibit a shift to more juvenile radiogenic isotopic compositions west of ~114°W longitude, but no shift in composition east of ~114°W longitude (Fig. 6A). Hf isotopic compositions of samples <40 Ma are most negative at 109°W to 111°W longitude and Nd isotopic compositions of samples <40 Ma are most negative at 112°W to 115°W longitude.

Nd and Hf isotopic composition can vary with whole rock composition. No chemical data were collected for the new samples in this study, but when compiled Nd isotopic data are plotted by whole rock SiO_2 content (Fig. 7B), the most mafic samples tend to have the highest values within a ~10 epsilon unit range, which is similar to the magnitude (*y*-axis range) of the "<40 Ma" and ">40 Ma" bands in Figure 6A. The total longitudinal (spatial) isotopic range in Figures 6A and 7B is larger (~30 epsilon units) than the ~10 epsilon unit isotopic range at any single longitude associated with changes in rock composition.

In addition to mean $\varepsilon Hf_{(t)}$ values corresponding to rock crystallization age, single-grain Lu-Hf isotopic analyses of inherited zircon age domains were obtained on domains identified during previous U-Pb analyses (Supplemental Table DR2). Zircon $\varepsilon Hf_{(t)}$ results for samples with Proterozoic ages from inherited cores are plotted in Figure 5 and grouped by crustal province. The data set is not comprehensive, but zircon grains from the same province generally fall along similar $^{176}Lu/^{177}Hf = 0.015$ crustal evolution lines, excluding the Mojave province. Some analyses from the Mojave province appear to have either evolved from a more compatible (higher Lu/Hf) source (i.e., shallower slope of an evolution line in ε-space) or to have experienced significant isotopic mixing with a more juvenile component during Phanerozoic crystallization. Hf model ages, based on the crustal evolution lines in Figure 5, for samples in the Grenville and Mazatzal provinces are generally consistent with published Nd model ages (Bennett and DePaolo, 1987), however, the Hf crustal model age for Yavapai province is older than equivalent Nd model ages (cf., Fig. 1). Because model ages are calculated based on composition of the material analyzed, there is no conversion required between Nd and Hf model ages. Note that Hf model ages based on zircon (e.g., Lu/Hf = 0.001) rather than crustal compositions are much older.

4.3. Zircon $\delta^{18}O$ Results

Results of zircon $\delta^{18}O$ analyses are presented in Table 1, Figures 4C and 6B, and Table DR3. Reported weighted mean zircon $\delta^{18}O$ values are calculated from age domains in zircon grains that are interpreted to reflect the crystallization/emplacement age of the sample, based on CL images and prior U-Pb analyses. Most samples have uncertainties of <1‰ for weighted mean values (Table 1). Like the zircon $\varepsilon Hf_{(t)}$ results, there is no clear temporal trend in $\delta^{18}O_{zrc}$ data apart from a subtle increase in the range of $\delta^{18}O$ values and increase in the mean $\delta^{18}O$ value toward the present (Fig. 4C).

Temporal trends are more apparent when the data are plotted against longitude (Fig. 6B). East of ~114°W longitude, all of the samples analyzed have mantle-like $\delta^{18}O_{zrc}$, although only one sample (Dragoon) older than 40 Ma was analyzed. West of ~114°W longitude, samples younger than 40 Ma display a shift to higher $\delta^{18}O$ (Fig. 6B) at any specific longitude. This shift is not well-defined (only two samples <40 Ma are located west of ~114°W longitude), but the shift is consistent with previously published oxygen isotopic data (Fig. 6B; Table DR4).

Except for samples Dragoon and Cooke, premagmatic zircon age domains were not systematically analyzed for $\delta^{18}O_{zrc}$. Premagmatic age domains in sample Dragoon yielded relatively high $\delta^{18}O_{zrc}$ values (8.8 ± 1.4‰; n = 4; Table DR3) relative to zircon rims (6.6 ± 1.6‰; Table 1). Premagmatic age domains in sample Cooke yielded relatively low $\delta^{18}O_{zrc}$ values (3.0

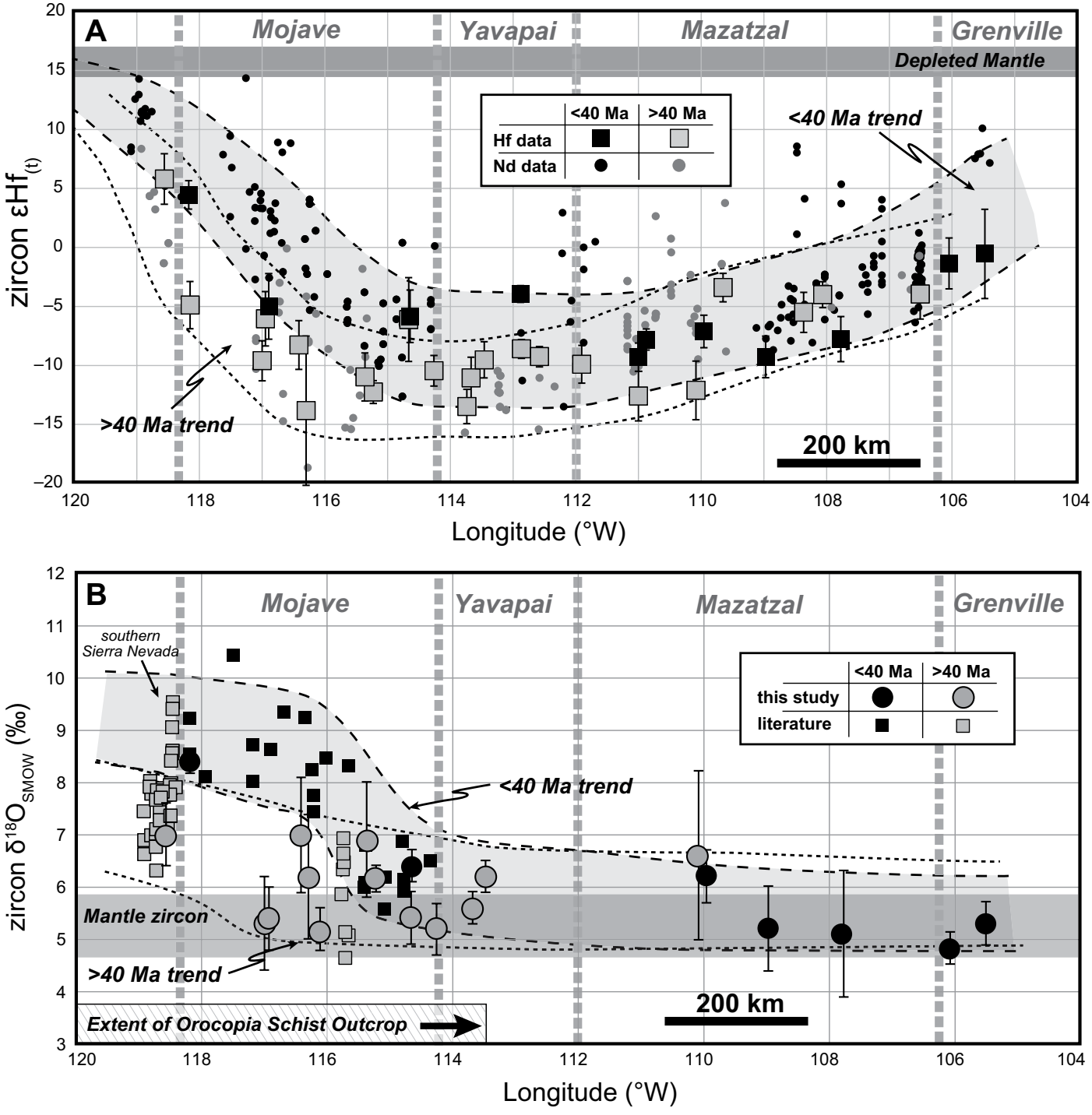

Figure 6. Plots of longitude (sub-parallel to orogenic structural grain) versus (A) mean zircon $\varepsilon Hf_{(t)}$ and (B) mean $\delta^{18}O_{zrc}$ from this study (Table 1). Uncertainties are 2σ for $\varepsilon Hf_{(t)}$ and 2 standard error (SE) for $\delta^{18}O_{zrc}$. Samples are grouped according to whether their age is older or younger than 40 Ma, which is the transition from a convergent to extensional tectonic regime at the end of the Laramide orogenic event (Constenius et al., 2003). Compiled whole rock $\varepsilon Nd_{(t)}$ data in panel A is converted to equivalent εHf values using the terrestrial array of Vervoort et al. (1999). Compiled $\delta^{18}O$ data in panel B come from whole rock and minerals other than zircon and are converted to equivalent $\delta^{18}O_{zrc}$ (see text for details). Compiled data are available in Table DR4 (see footnote 1). Error bars for $\delta^{18}O_{zrc}$ data are sometimes smaller than the symbol.

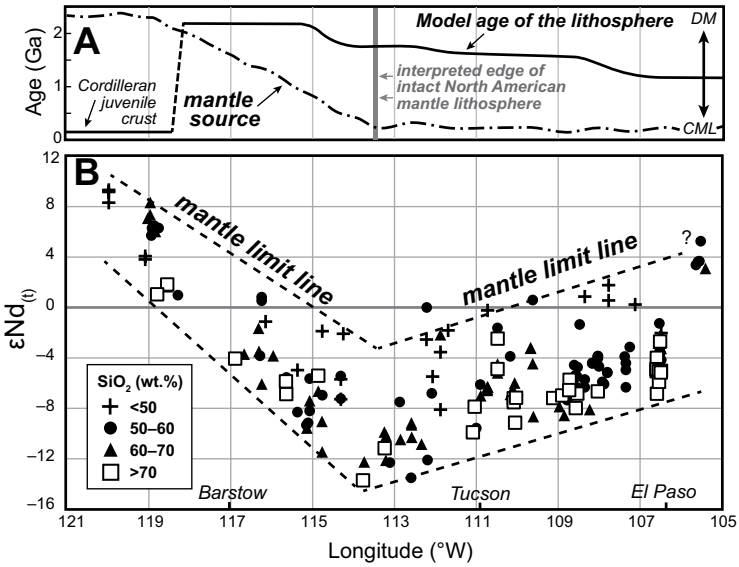

Figure 7. (A) Plot of longitude versus lithospheric province model age (Nd or Hf) (solid line; Fig. 1) and interpreted upper mantle source (dash-dot line). The upper mantle is interpreted to vary between a predominately depleted mantle (DM) source and a continental mantle lithosphere (CML) source and the (dash-dot) line for the interpreted mantle source is a proxy for the inferred geometry of the lithosphere-asthenosphere boundary (LAB). The western extent of intact mantle lithosphere is estimated based on the change in slope of the mantle limit lines in panel B. (B) Plot of longitude versus compiled whole rock $\varepsilon Nd_{(t)}$ of samples from the southwestern U.S. Cordillera, grouped by SiO_2 (wt%). The isotopic composition of the mantle source can be estimated by examining the most mafic samples and drawing a mantle limit line (Miller et al., 2000; Chapman et al., 2017). Samples with ages of 15–110 Ma are shown to illustrate the use of mantle limit lines. Changes in the inferred position of the LAB could be refined by using smaller increments of time, as in Figure 6. Compiled data are available in Table DR4 (see footnote 1).

± 0.4‰; n = 2; Table DR3) relative to zircon rims (5.1 ± 1.2‰; Table 1). Analysis of inherited zircon age domains in samples Dragoon and Cooke yielded U-Pb ages of 1.5–1.6 Ga (Table DR1), which may be associated with the premagmatic $\delta^{18}O_{zrc}$ values, although the domains analyzed for oxygen isotopes were not directly dated by U-Pb.

5. DISCUSSION

5.1. The Origin of Spatial Trends in Radiogenic Isotope Data

Before attempting to interpret the isotopic results in terms of tectonic events or geodynamic processes, the origin of the spatial trends needs to be evaluated. End-members for factors that could generate the spatial trends in the Hf and Nd isotopic composition of igneous rocks in Figure 6A are: (1) spatial changes in the degree of crustal (or sediment) assimilation; (2) spatial changes in the isotopic composition of the material assimilated; and (3) spatial changes in the melt source. Except for Laramide-age peraluminous rocks associated with crustal anatexis (Miller and Barton, 1990), the initial melt source for Mesozoic and younger Cordilleran (continental arc) magmatism is interpreted to be the upper mantle (e.g., Farmer and DePaolo, 1984; Hildreth and Moorbath, 1988; Annen et al., 2006). Thus, estimating the isotopic composition of the mantle source can help to distinguish between the end-members listed above.

The radiogenic isotopic composition of the mantle source can be estimated by examining the most primitive or least differentiated (e.g., lowest SiO_2 wt%) rocks from a particular magmatic suite (Coleman and Glazner, 1997) (Fig. 7B). The most positive $\varepsilon Nd_{(t)}$ values in Figure 7B can be used as "mantle limit lines" (cf., Miller et al., 2000; Chapman et al., 2017) to help constrain the isotopic composition of the mantle source region. The top of the ">40 Ma" and "<40 Ma" bands in Figure 6A are not strictly mantle limit lines (sensu Miller et al., 2000), but their geometry provides a crude approximation to the mantle isotopic composition. Mantle limit lines that incorporate all data points (sensu Miller et al., 2000) could be drawn on Figure 6A by increasing the top of the "40 Ma" bands by 5–10 epsilon units.

If the longitudinal variation in $\varepsilon Hf_{(t)}$ and $\varepsilon Nd_{(t)}$ in the southwestern U.S. Cordillera was related only to spatial changes in the efficiency of crustal assimilation (end-member 1) or only related to isotopic variations in the crust (i.e., basement terranes) (end-member 2), then the mantle limit lines in Figure 7B, or the top of the "40 Ma" bands in Figure 6A, would be expected to be flat (reflecting a single mantle source), rather than sub-parallel to the most negative $\varepsilon Nd_{(t)}$ and $\varepsilon Hf_{(t)}$ values in the isotopic trends in Figures 6A and 7B. Furthermore, Figure 7B shows that there is a wide range of rock compositions (SiO_2 wt%) at all longitudes. If the radiogenic spatial trends were only related to crustal assimilation, then the most mafic samples would be expected to occur in the regions with the highest $\varepsilon Nd_{(t)}$ or $\varepsilon Hf_{(t)}$ values. The isotopic variation at any specific longitude (≤10 epsilon units) is primarily related to assimilation of crustal material (Fig. 7B), but the range of the spatial radiogenic isotopic trend across all longitudes (~30 epsilon units) is too large to be explained by changes in the degree of crustal assimilation alone (end-member 1). These observations are consistent with previous studies of the southwestern U.S. Cordillera that suggested spatial trends in isotopic composition principally reflect the composition of the mantle source (Miller et al., 2000; Chapman et al., 2017).

5.2. Mantle Sources

The importance of the mantle source in controlling spatial radiogenic isotopic trends is supported by individual isotopic studies from the southwestern U.S. Cordillera that indicate that, prior to late Miocene lithospheric (Basin and Range) extension, the North American mantle lithosphere remained coupled to the crust and was the primary source of magmatism (Farmer et al., 1995, 2008; DePaolo and Daley, 2000; McMillan et al., 2000). In general, these studies use the evolved radiogenic isotopic compositions of relatively primitive (mafic) igneous rocks infer an evolved mantle source (i.e., the mantle lithosphere).

During Basin and Range extension (ca. 15 Ma to present) there was a widespread shift to more juvenile radiogenic and oxygen isotopic compositions that is attributed to a change in the mantle source region from continental mantle

lithosphere to asthenospheric mantle (from isotopically enriched to depleted) as extension progressed (Glazner et al., 1991; Farmer et al., 1995; DePaolo and Daley, 2000; McMillan et al., 2000). These studies provide a base-line for recognizing melts originating in the asthenospheric (depleted) mantle and suggest that prior to Basin and Range extension the mantle lithosphere in many places in the southwestern U.S. Cordillera was largely intact. Dismemberment or removal of mantle lithosphere from the southwestern U.S. Cordillera during the late Miocene to recent was not uniform and in some locations evolved radiogenic isotopes suggest that ancient mantle lithosphere is still preserved in the Basin and Range province (Farmer et al., 1989).

5.2.1. East of ~114°W Longitude

The relationship between the lithosphere and the isotopic composition magmatism is most pronounced on the eastern side (east of ~114°W longitude) of the U-shaped $\varepsilon Hf_{(t)}$ spatial trend in Figure 6A. The eastward increase in $\varepsilon Hf_{(t)}$ values mirrors a decrease in basement terrane U-Pb ages and Sm-Nd model ages (Bennett and DePaolo, 1987; Whitmeyer and Karlstrom, 2007) (Fig. 7A). Moreover, $\varepsilon Hf_{(t)}$ values associated with Proterozoic inherited ages (e.g., some zircon cores) and crystallization ages of samples from the Yavapai, Mazatzal, and Grenville crustal provinces (located east of ~114°W longitude) plot along crustal Lu/Hf evolution lines (Fig. 5), which is consistent with melting and assimilation of a lithospheric source of approximately the same age and composition as the lithospheric province exposed at the surface. These observations suggest that the spatial radiogenic isotopic trend east of ~114°W longitude is primarily related to the age and composition of the lithosphere (including mantle lithosphere).

5.2.2. West of ~114°W Longitude

The nature of mantle sources is also important for interpreting the spatial radiogenic isotopic trend west of ~114°W longitude (Fig. 6A). The Mojave terrane located west of ~114°W longitude has the oldest crustal model ages in the southwestern U.S. Cordillera (Wooden et al., 2013; Fig. 1), but $\varepsilon Hf_{(t)}$ values of samples from the Mojave terrane are less evolved than expected (<–15 $\varepsilon Hf_{(t)}$) if Mesozoic to Cenozoic igneous rocks were derived from an ancient lithospheric source (the explanation for the spatial isotopic trend east of ~114°W longitude). In addition, Lu-Hf analyses of Mesozoic to Cenozoic zircon age domains do not plot along crustal evolution lines with Proterozoic zircon age domains from the same grain or sample from the Mojave terrane (Fig. 5). Part of this inconsistency likely reflects complexity in the evolution of the Mojave province (Wooden et al., 2013), but samples >40 Ma and <40 Ma both show a westward increase in zircon $\varepsilon Hf_{(t)}$, which is consistent with existing whole rock Nd and Sr isotopic data from the Mojave region (Glazner and O'Neil, 1989; Miller et al., 2000) (Fig. 6A).

Previous studies have suggested that this westward transition to more juvenile isotopic values reflects a transition from continental mantle lithosphere to juvenile depleted asthenosphere or oceanic mantle lithosphere as the mantle source (Glazner and O'Neil, 1989; Miller et al., 2000; Chapman et al., 2017). Chapman et al. (2017) suggested that this transition in the southwest U.S. Cordillera is an intrinsic feature of continental arcs and Cordilleran orogens globally and reflects systematic removal of mantle lithosphere and possibly lower crust close to the subduction interface.

5.3. Temporal Trends in Radiogenic Isotopic Data

Following the above interpretations, the change in slope (from negative to positive) of the $\varepsilon Hf_{(t)}$ and $\varepsilon Nd_{(t)}$ trends in Figure 6A can be used to roughly estimate the position of the edge of intact North America mantle lithosphere and how that feature may have changed through time. For samples older than 40 Ma, the lowest $\varepsilon Hf_{(t)}$ values, and interpreted western edge of intact continental mantle lithosphere, occur at 117°W to 116°W longitude (Fig. 6A). West of this longitude, the mantle lithosphere is interpreted to have gradually thinned toward the trench, consistent with previous isotopic studies that suggested the mantle lithosphere was thin to absent in the westernmost Mojave region during the Jurassic (Miller et al., 1995; Miller and Glazner, 1995) (Figs. 2A, 2B). South of the study area, evolved isotope ratios suggest that continental mantle lithosphere extended to at least the present-day location of the San Andreas fault during the Late Cretaceous (Barth et al., 2016). Dense sampling of the Peninsular Ranges batholith (on the west side of the San Andreas fault, Fig. 1) indicates that during the Cretaceous, the transition to more juvenile isotopic compositions occurred across a horizontal distance of as little as ~50 km at this location (Kistler et al., 2003).

Continental mantle lithosphere was the likely source for Jurassic igneous rocks east of ~116°W longitude (e.g., Rämö et al., 2002) (Fig. 2A). The approximate western edge of intact mantle lithosphere after 40 Ma is interpreted to be located between 114°W and 113°W longitude (Figs. 2C and 7). Previous isotopic studies of volcanic rocks in the Mojave region suggested that the western edge of intact mantle lithosphere extended to ~116°W longitude during the early to middle Miocene (Glazner and O'Neil, 1989; Miller et al., 2000). The shift in the position of the western edge of intact North American mantle lithosphere suggests that a large segment (200–400 km in width, not restored for contraction or extension) of the mantle lithosphere was thinned and/or removed by 40 Ma. The thin dashed line labeled, "future LAB" in cross-section X (Fig. 2B) marks the region of the mantle lithosphere and possibly lower crust that is hypothesized to have been removed during the Laramide orogeny. Cross-section Y (Fig. 2C) shows the position of the edge of intact mantle lithosphere (heavy vertical dashed line) has shifted eastward in comparison to cross-section X. The loss or partial removal of mantle lithosphere has been previously associated with low-angle to flat-slab subduction during the Laramide orogeny (Miller et al., 2000; Saleeby, 2003). Surface exposures of the Pelona–Orocopia–Rand schist (associated with Laramide shallow subduction) occur as far east as ~113.5°W (Fig. 6B; Chapman, 2017), comparable to the estimated western edge of post–40 Ma intact mantle lithosphere (Figs. 2C, 2D).

5.4. Zircon Oxygen Isotopes

Similar to the radiogenic isotopic data, there are differences in zircon oxygen isotopes east and west of ~114°W longitude and before and after ca. 40 Ma. East of ~114°W longitude, all of the samples analyzed have mantle-like $\delta^{18}O_{zrc}$ (Fig. 6B), consistent with a mantle source (Eiler, 2001) that is interpreted to be the continental mantle lithosphere and suggests limited assimilation of crustal material. There paucity of samples >40 Ma located east of ~114°W longitude make it difficult to assess temporal changes, but it appears as if there is little difference in $\delta^{18}O_{zrc}$.

West of ~114°W longitude, $\delta^{18}O_{zrc}$ generally decreases from west to east (Fig. 6B). This contrasts with the central U.S. Cordillera where $\delta^{18}O_{zrc}$ generally increases from west to east (King et al., 2004). In the central U.S. Cordillera, oxygen isotope ratios increase east of the $^{87}Sr/^{86}Sr = 0.706$ line and high $\delta^{18}O_{zrc}$ is believed to be related to assimilation of crustal material (King et al., 2004). The highest $\delta^{18}O_{zrc}$ values in the central U.S. Cordillera correspond to the regions with the thickest Paleozoic passive margin sequence (Cordilleran miogeocline; Stewart, 2005) and $\delta^{18}O_{zrc}$ was slightly higher during the Cretaceous, when the crust is believed to have been the thickest, which may favor crustal assimilation (King et al., 2004). The Cordilleran miogeocline is present in the

westernmost Mojave region (Stewart, 2005) and correlates with the position of the highest $\delta^{18}O$ in the southwestern U.S. Cordillera prior to 40 Ma (Figs. 2B and 6B). Values of $\delta^{18}O$ for igneous rocks older than 40 Ma in the Mojave region are only slightly higher than mantle values (Fig. 6B). The spatial pattern of $\delta^{18}O$ in the Sierra Nevada is more complex (Lackey et al., 2008) and particularly high $\delta^{18}O_{zrc}$ (>8‰) in the southern Sierra Nevada (Fig. 6B) has been attributed to underthrust altered oceanic and volcanic crust during exotic terrane accretion (Lackey et al., 2005).

There is a pronounced temporal shift to higher $\delta^{18}O$ after ca. 40 Ma in samples located west of ~114°W longitude (Fig. 6B). Glazner and O'Neil (1989) suggested that high whole rock $\delta^{18}O$ (equivalent to >8‰ $\delta^{18}O_{zrc}$, calibrated for the SiO_2 wt% of the whole rock; Lackey et al., 2008) for Miocene volcanic rocks west of ~116°W longitude was caused by melting and assimilation of underplated Pelona–Orocopia–Rand schist. The Pelona–Orocopia–Rand schist has relatively juvenile $\varepsilon Nd_{(t)}$ compositions and relatively heavy $\delta^{18}O$ compositions (Glazner and O'Neil, 1989). The results of this study are consistent with that interpretation and indicate that Mesozoic to early Cenozoic igneous rocks in the Mojave region are characterized by relatively lower $\delta^{18}O_{zrc}$ (≤7‰) (Fig. 6B). Because the Pelona–Orocopia–Rand sediments were emplaced before ca. 40 Ma (Grove et al., 2003), the relatively heavy $\delta^{18}O$ of Miocene rocks is likely related to partial melting and assimilation of Pelona–Orocopia–Rand schist in the lower crust, rather than introduction of high $\delta^{18}O$ material into the mantle source region during subduction. Also, because Miocene igneous rock suites in the Mojave are metaluminous and extend to mafic compositions (Miller et al., 2000), single-stage melting of the Pelona–Orocopia–Rand schist (crustal anatexis), without precursory partial melting of the mantle is unlikely.

5.5. Interpreting Isotopic Trends from Cordilleran Orogenic Systems

One of the central implications of this study is that the isotopic composition of igneous rocks in Cordilleran orogens may not always record changes in tectonic processes or geodynamics and that the age and composition of the lithosphere hosting the magmatic products should be considered. The absence of a temporal shift in isotopic compositions east of ~114°W longitude (Fig. 6) suggests that continental mantle lithosphere was the predominant mantle source for Mesozoic to early Miocene magmas. As magmatism migrated back and forth across the Cordillera east of ~114°W longitude (e.g., Fig. 3), the isotopic composition of magmatism at a specific geographic location remained relatively constant through time (Fig. 6A). Events that generated nearly contemporaneous magmatism at different longitudes, such as the ignimbrite flare-up, had isotopic values that reflect the age and composition of the local lithosphere. Variation in radiogenic isotopic composition at a specific geographic location is generally ≤10 $\varepsilon Nd_{(t)}$ and most of that variation appears related to differentiation and assimilation within the crust (Fig. 7B), which may be independent of the tectonic or geodynamic conditions at the time. Despite changes in subduction zone dynamics (low-angle subduction, slab-rollback, slab foundering) and a transition from a contractional to extensional tectonic regime, there are not large (>10 $\varepsilon Nd_{(t)}$) changes in the isotopic composition of magmatism east of ~114°W longitude.

Tectonic processes do appear to have influenced radiogenic and stable (oxygen) isotopic compositions west of ~114°W longitude (Fig. 6), but not in the ways envisioned by Kemp et al. (2009) for accretionary orogens, which have been applied to Cordilleran orogens such as the Andes (e.g., Boekhout et al., 2015). A shift to more juvenile radiogenic isotopes west of ~114°W longitude for samples <40 Ma suggests that the mantle lithosphere was thinned or partially removed and replaced by depleted mantle (presumably either asthenosphere or young oceanic mantle lithosphere). This shift is not directly related to periods of extension or crustal thinning. These results suggest that crustal processes that do not involve removal or modification of the mantle lithosphere (e.g., crustal shortening and thickening) may not be easily resolvable in the radiogenic isotopic record.

Zircon $\delta^{18}O$ data from west of ~114°W longitude may also not be directly related to tectonic processes. The relatively large (2–4‰) post–40 Ma shift to heavier $\delta^{18}O$ (Fig. 6B) is interpreted to reflect extensive underplating of sediment during shallow subduction (Fig. 2). Crustal thickening accompanied shallow subduction during the Laramide orogeny and may have enhanced crustal assimilation, leading to larger $\delta^{18}O_{zrc}$ values, but periods of contraction in Cordilleran orogens are not always associated with low-angle subduction or sediment underplating. Smaller variations in $\delta^{18}O_{zrc}$ (≤2‰) may be related to the degree of crustal assimilation, however, spatial variations in $\delta^{18}O$ (e.g., increas-

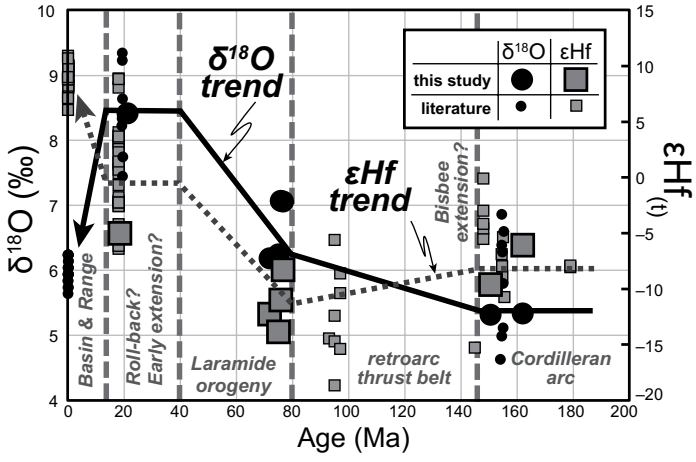

Figure 8. Isotopic data from the central Mojave region, southwestern U.S. Cordillera, (~115.5–117°W longitude, a subset of the entire Mojave province). Plot of age versus mean zircon $\varepsilon Hf_{(t)}$ and mean $\delta^{18}O_{zrc}$ for samples analyzed in this study (Table 1) and compiled whole rock $\varepsilon Nd_{(t)}$ (converted to zircon $\varepsilon Hf_{(t)}$) and $\delta^{18}O$ data. Conversion of compiled data is the same as in Figure 6 and is available in Table DR4 (see footnote 1). Increases in zircon $\varepsilon Hf_{(t)}$ and $\delta^{18}O_{zrc}$ during the Late Cretaceous to early Miocene are attributed to partial removal and replacement of the continental mantle lithosphere with depleted asthenospheric mantle or oceanic lithosphere during the Laramide orogeny (Miller et al., 2000) and assimilation of underplated Pelona–Orocopia–Rand schist (Fig. 2) (Glazner and O'Neil, 1989). Temporal shifts to more juvenile zircon $\varepsilon Hf_{(t)}$ and mantle-like $\delta^{18}O_{zrc}$ values during the late Miocene to present are related to Basin and Range lithospheric extension and increasingly asthenospheric melt sources.

ing $\delta^{18}O$ toward the trench; Fig. 6B) appear to be pronounced for samples >40 Ma as well.

The results of this study suggest that the geographic distribution of magmatism should be considered when interpreting tectonic events or geodynamic processes from igneous isotopic data. Detrital isotopic data (e.g., zircon Lu-Hf) may be particularly susceptible to misinterpretation. For example, during the Laramide orogeny in the southwestern U.S. Cordillera the locus of magmatism migrated eastward into increasingly isotopically juvenile crustal provinces. This was a period of contraction and crustal thickening, however, zircon $\varepsilon Hf_{(t)}$ data from this event would record a temporal trend to more juvenile compositions.

The best way to interpret specific tectonic events from isotopic data may be to focus on a limited geographic area that is less likely to be affected by regional isotopic trends. We present such an analysis for the Mojave Desert region in Figure 8 (~114°W to 118°W longitude). During the Jurassic to Late Cretaceous, the radiogenic isotopic composition of magmatism was relatively evolved, reflecting an enriched continental mantle lithosphere source, consistent with mantle-like or mildly evolved zircon oxygen isotope ratios (<7‰ $\delta^{18}O_{zrc}$). The slightly more negative $\varepsilon Hf_{(t)}$ in the Late Cretaceous, compared to the Jurassic and Early Cretaceous (Fig. 8), may reflect more efficient crustal assimilation in thicker crust associated with retroarc shortening (Spencer and Reynolds, 1990). Alternatively, these shifts may reflect changes in the lithospheric mantle source, changes within the Mojave province lower crust, or changes at the crust-mantle boundary, as the arc evolved (Barth and Wooden, 2010; Barth et al., 2016). Slightly higher $\delta^{18}O_{zrc}$ in the Late Cretaceous is also consistent with more efficient crustal assimilation. During the Laramide orogeny, the North American mantle lithosphere (radiogenically enriched peridotite) in the Mojave Desert region is interpreted to have been at least partially replaced by young oceanic lithosphere (isotopically depleted mafic crust and peridotite) or asthenospheric mantle (isotopically depleted peridotite) (Miller et al., 2000) (Figs. 2C, 2D), causing $\varepsilon Hf_{(t)}$ to increase in early Miocene igneous rocks (Fig. 8). A concurrent increase in $\delta^{18}O$ in the Mojave Desert region is interpreted to reflect partial melting and assimilation of Pelona–Orocopia–Rand schist within the lower crust (Glazner and O'Neil, 1989) (Figs. 2D and 8). During the early Miocene to the Quaternary, $\delta^{18}O$ returns to mantle-like compositions (~5–6‰) and radiogenic isotope ratios shift to more isotopically juvenile compositions (~+10 $\varepsilon Hf_{(t)}$), both of which are consistent with partial melting of the asthenospheric mantle with minimal crustal assimilation during Basin and Range lithospheric extension (Glazner et al., 1991) (Fig. 8).

6. CONCLUSIONS

This study is the first regional zircon $\varepsilon Hf_{(t)}$ and $\delta^{18}O_{zrc}$ data set for Mesozoic to early Miocene igneous rocks in the southwestern U.S. Cordillera. We recognize orogen-scale spatial and temporal isotopic trends, interpret the origin of those trends, and integrate the isotopic data into the geologic history of the region. The results are used to evaluate and improve the use of zircon isotopic data to interpret tectonic events and geodynamics processes in Cordilleran orogens.

When plotted against longitude (sub-parallel to the orogenic structural grain) zircon $\varepsilon Hf_{(t)}$ data form a U-shaped isotopic trend with a minimum at ~114°W longitude and increases toward the east and west (Fig. 6A). The eastern limb of the U-shaped zircon $\varepsilon Hf_{(t)}$ trend is interpreted to reflect an eastward decrease in the age of lithospheric provinces (Figs. 1 and 7A). Zircon $\varepsilon Hf_{(t)}$ from inherited cores plot along mean crustal Lu/Hf evolution lines (Fig. 5), consistent with partial melting of the same lithospheric source through time. Zircon $\delta^{18}O$ east of ~114°W longitude is similar in composition to mantle-derived zircon and indicates limited crustal assimilation in Mesozoic to recent igneous rocks (Fig. 6B). Correlation of whole rock SiO_2 (wt%) with radiogenic isotope ratios (Fig. 7B) suggests that the continental mantle lithosphere was the mantle source for the majority of Mesozoic to early Miocene igneous rocks in the eastern limb of the U-shaped trend (Fig. 2). East of ~114°W longitude, there is no significant oxygen or Hf isotope difference between magmatism associated with shallow to flat-slab subduction and crustal thickening during the Laramide orogeny and magmatism associated with subduction roll-back or foundering of the Farallon slab and crustal extension following the Laramide orogeny (Fig. 2). These results indicate that subduction dynamics and orogenic processes may not always be resolvable in the zircon $\varepsilon Hf_{(t)}$ record. The largest temporal changes in zircon $\varepsilon Hf_{(t)}$ are related to the migration of magmatism into different lithospheric provinces (basement terranes) rather than periods of contraction or extension.

The western limb of the U-shaped zircon $\varepsilon Hf_{(t)}$ trend (Fig. 6A) is interpreted to reflect a transition from intact North American continental mantle lithosphere in the east to a depleted asthenospheric or oceanic lithospheric mantle source region in the west (Figs. 2 and 7A). The minimum, or change in slope, of the U-shaped trend (Fig. 6A) is used to estimate the position of the western edge of intact continental mantle lithosphere through time (Fig. 2, heavy dashed vertical line in cross sections W–Z). Prior to the Laramide orogeny (>40 Ma), the edge of intact mantle lithosphere was located at 116–117°W longitude (present-day coordinates) (Figs. 2A, 2B, and 6A). There is a shift to more juvenile zircon $\varepsilon Hf_{(t)}$ for samples <40 Ma and the minimum of the U-shaped isotopic trend moves eastward. The <40 Ma isotopic shift is attributed to partial removal or replacement of a portion of the continental mantle lithosphere in the Mojave region during the Laramide orogeny and the edge of intact continental mantle is interpreted to have moved to ~114°W longitude (present-day coordinates) (Figs. 2C, 2D, and 6A). There is also a shift to significantly higher $\delta^{18}O$ in samples younger than 40 Ma, which is attributed to lower crustal assimilation of Pelona–Orocopia–Rand schist that was underplated during the Laramide orogeny (Figs. 2C, 2D, and 6B). These results suggest that changes in the composition of the upper mantle (e.g., from evolved continental mantle lithosphere to depleted asthenospheric mantle) have the greatest influence on the radiogenic isotopic composition of Cordilleran magmatism. The influence of crustal processes, like thickening or thinning, are less pronounced and may be obscured by spatial trends or differences in the efficiency or amount of crustal assimilation, which may be responsible for ≤10 zircon $\varepsilon Hf_{(t)}$ shifts at any specific location in the orogen.

The isotopic data from the southwestern U.S. Cordillera show that spatial and temporal zircon isotopic trends can be an effective tool to monitor changes in the composition or architecture of the mantle source region and have applications for interpreting past geodynamic processes such as subduction erosion, delamination of the mantle lithosphere, and sediment underplating. However, regional (spatial) trends in isotopic composition related to lithospheric composition are significantly larger than temporal trends associated with tectonic processes in both the mantle and crust. Distinguishing tectonic events from arc migration in Cordilleran orogens using detrital zircon data sets is particularly difficult without information on the sediment source area. Limiting the geographic scope of zircon isotopic investigations (Fig. 8) is one way to help avoid conflating spatial and temporal isotopic trends.

ACKNOWLEDGEMENTS

Funding was provided by an EarthScope award for Geochronology Student Research (AGeS) (J.C.), a University of Arizona Graduate and Professional Student Council (GPSC) grant (J.C.), NSF EAR 1725002 (M.N.D), and the Romanian Executive

Agency for Higher Education, Research, Development and Innovation Funding project PN-III-P4-ID-PCE-2016-0127 (M.N.D.). Support for the University of Arizona LaserChron Center comes from the National Science Foundation Division of Earth Sciences (NSF EAR) 1338583 and NSF EAR 1649254 (G.G.). WiscSIMS is supported by NSF EAR 1355590, NSF EAR 1658823, and University of Wisconsin–Madison (J.V.). J.D. Mizer provided zircon mounts for previously dated samples. Constructive reviews and comments from editor Aaron Cavosie, associate editor Chris Kirkland, Jon Spencer, Andy Barth, and Paul Wetmore helped to improve the manuscript.

REFERENCES CITED

Annen, C., Blundy, J.D., and Sparks, R.S.J., 2006, The genesis of intermediate and silicic magmas in deep crustal hot zones: Journal of Petrology, v. 47, no. 3, p. 505–539, https://doi.org/10.1093/petrology/egi084.

Armstrong, R.L., and Ward, P., 1991, Evolving geographic patterns of Cenozoic magmatism in the North American Cordillera: The temporal and spatial association of magmatism and metamorphic core complexes: Journal of Geophysical Research. Solid Earth, v. 96, p. 13201–13224, https://doi.org/10.1029/91JB00412.

Atwater, T., and Stock, J., 1998, Pacific-North America plate tectonics of the Neogene southwestern United States: An update: International Geology Review, v. 40, p. 375–402, https://doi.org/10.1080/00206819809465216.

Balgord, E.A., 2017, Triassic to Neogene evolution of the south-central Andean arc determined by detrital zircon U-Pb and Hf analysis of Neuquén Basin strata, central Argentina (34°S–40°S): Lithosphere, v. 9, p. 453–462, https://doi.org/10.1130/L546.1.

Barth, A.P., and Wooden, J.L., 2006, Timing of magmatism following initial convergence at a passive margin, southwestern US Cordillera, and ages of lower crustal magma sources: The Journal of Geology, v. 114, no. 2, p. 231–245, https://doi.org/10.1086/499573.

Barth, A.P., and Wooden, J.L., 2010, Coupled elemental and isotopic analyses of polygenetic zircons from granitic rocks by ion microprobe, with implications for melt evolution and the sources of granitic magmas: Chemical Geology, v. 277, p. 149–159, https://doi.org/10.1016/j.chemgeo.2010.07.017.

Barth, A.P., Wooden, J.L., Jacobson, C.E., and Probst, K., 2004, U-Pb geochronology and geochemistry of the McCoy Mountains Formation, southeastern California: A Cretaceous retroarc foreland basin: Geological Society of America Bulletin, v. 116, no. 1-2, p. 142–153, https://doi.org/10.1130/B25288.1.

Barth, A.P., Wooden, J.L., Mueller, P.A., and Economos, R.C., 2016, Granite provenance and intrusion in arcs: Evidence from diverse zircon types in Big Bear Lake Intrusive Suite, USA: Lithos, v. 246, p. 261–278, https://doi.org/10.1016/j.lithos.2015.12.009.

Barth, A.P., Wooden, J.L., Miller, D.M., Howard, K.A., Fox, L.K., Schermer, E.R., and Jacobson, C.E., 2017, Regional and temporal variability of melts during a Cordilleran magma pulse: Age and chemical evolution of the Jurassic arc, eastern Mojave Desert, California: Geological Society of America Bulletin, v. 129, p. 429–448, https://doi.org/10.1130/B31550.1.

Beard, B.L., and Johnson, C.M., 1997, Hafnium isotope evidence for the origin of Cenozoic basaltic lavas from the southwestern United States: Journal of Geophysical Research: Solid Earth, v. 102, p. 20149–20178, https://doi.org/10.1029/97JB01731.

Bennett, V.C., and DePaolo, D.J., 1987, Proterozoic crustal history of the western United States as determined by neodymium isotopic mapping: Geological Society of America Bulletin, v. 99, p. 674–685, https://doi.org/10.1130/0016-7606(1987)99<674:PCHOTW>2.0.CO;2.

Bindeman, I.N., and Valley, J.W., 2001, Low-$\delta^{18}O$ rhyolites from Yellowstone: Magmatic evolution based on analyses of zircons and individual phenocrysts: Journal of Petrology, v. 42, p. 1491–1517, https://doi.org/10.1093/petrology/42.8.1491.

Boekhout, F., Roberts, N.M., Gerdes, A., and Schaltegger, U., 2015, A Hf-isotope perspective on continent formation in the south Peruvian Andes, *in* Roberts, N., Van Kranendonk, M., Parman, S., Shirey, S., and Clift, P.D., eds., Continent Formation Through Time: Geological Society of London Special Publication 389, p. 305–321, https://doi.org/10.1144/SP389.6.

Bouvier, A., Vervoort, J.D., and Patchett, P.J., 2008, The Lu–Hf and Sm–Nd isotopic composition of CHUR: Constraints from unequilibrated chondrites and implications for the bulk composition of terrestrial planets: Earth and Planetary Science Letters, v. 273, p. 48–57, https://doi.org/10.1016/j.epsl.2008.06.010.

Busby, C.J., 2012, Extensional and Transtensional Continental Arc Basins: Case Studies from the Southwestern United States, *in* Busby, C., and Azor, A., eds., Tectonics of Sedimentary Basins: Recent Advances: Chichester, UK, John Wiley & Sons, Ltd., p. 382–404, https://doi.org/10.1002/9781444347166.ch19.

Cecil, M.R., Gehrels, G., Ducea, M.N., and Patchett, P.J., 2011, U-Pb-Hf characterization of the central Coast Mountains batholith: Implications for petrogenesis and crustal architecture: Lithosphere, v. 3, p. 247–260, https://doi.org/10.1130/L134.1.

Cecil, M.R., Rotberg, G.L., Ducea, M.N., Saleeby, J.B., and Gehrels, G.E., 2012, Magmatic growth and batholithic root development in the northern Sierra Nevada, California: Geosphere, v. 8, p. 592–606, https://doi.org/10.1130/GES00729.1.

Chapman, A.D., 2017, The Pelona–Orocopia–Rand and related schists of southern California: A review of the best-known archive of shallow subduction on the planet: International Geology Review, v. 59, p. 664–701, https://doi.org/10.1080/00206814.2016.1230836.

Chapman, J.B., Ducea, M.N., Kapp, P., Gehrels, G.E., and DeCelles, P.G., 2017, Spatial and temporal radiogenic isotopic trends of magmatism in Cordilleran orogens: Gondwana Research, v. 48, p. 189–204, https://doi.org/10.1016/j.gr.2017.04.019.

Clinkscales, C.A., and Lawton, T.F., 2015, Timing of Late Cretaceous shortening and basin development, Little Hatchet Mountains, southwestern New Mexico, USA–implications for regional Laramide tectonics: Basin Research, v. 27, p. 453–472, https://doi.org/10.1111/bre.12083.

Coleman, D.S., and Glazner, A.F., 1997, The Sierra Crest magmatic event: Rapid formation of juvenile crust during the Late Cretaceous in California: International Geology Review, v. 39, p. 768–787, https://doi.org/10.1080/00206819709465302.

Coney, P.J., and Reynolds, S.J., 1977, Cordilleran benioff zones: Nature, v. 270, p. 403–406, https://doi.org/10.1038/270403a0.

Constenius, K.N., Esser, R.P., and Layer, P.W., 2003, Extensional collapse of the Charleston-Nebo salient and its relationship to space-time variations in Cordilleran orogenic belt tectonism and continental stratigraphy, *in* Raynolds, R.G. and Flores, R.M., eds., Cenozoic Systems of the Rocky Mountain Region: Denver, Colorado, Rocky Mountain Section SEPM, p. 303–353.

Davis, G.H., 1979, Laramide folding and faulting in southeastern Arizona: American Journal of Science, v. 279, p. 543–569, https://doi.org/10.2475/ajs.279.5.543.

DeCelles, P.G., 2004, Late Jurassic to Eocene evolution of the Cordilleran thrust belt and foreland basin system, western USA: American Journal of Science, v. 304, p. 105–168, https://doi.org/10.2475/ajs.304.2.105.

DeCelles, P.G., and Graham, S.A., 2015, Cyclical processes in the North American Cordilleran orogenic system: Geology, v. 43, p. 499–502, https://doi.org/10.1130/G36482.1.

DeCelles, P.G., Ducea, M.N., Kapp, P., and Zandt, G., 2009, Cyclicity in Cordilleran orogenic systems: Nature Geoscience, v. 2, p. 251, https://doi.org/10.1038/ngeo469.

DePaolo, D.J., and Daley, E.E., 2000, Neodymium isotopes in basalts of the southwest basin and range and lithospheric thinning during continental extension: Chemical Geology, v. 169, p. 157–185, https://doi.org/10.1016/S0009-2541(00)00261-8.

Dickinson, W.R., 1991, Tectonic setting of faulted Tertiary strata associated with the Catalina core complex in southern Arizona: Geological Society of America Special Paper 264, 106 p., https://doi.org/10.1130/SPE264.

Dickinson, W.R., 2004, Evolution of the North American Cordillera: Annual Review of Earth and Planetary Sciences, v. 32, p. 13–45, https://doi.org/10.1146/annurev.earth.32.101802.120257.

Dickinson, W.R., and Lawton, T.F., 2001a, Tectonic setting and sandstone petrofacies of the Bisbee basin (USA–Mexico): Journal of South American Earth Sciences, v. 14, p. 475–504, https://doi.org/10.1016/S0895-9811(01)00046-3.

Dickinson, W.R., and Lawton, T.F., 2001b, Carboniferous to Cretaceous assembly and fragmentation of Mexico: Geological Society of America Bulletin, v. 113, p. 1142–1160, https://doi.org/10.1130/0016-7606(2001)113<1142:CTCAAF>2.0.CO;2.

Dickinson, W.R., Klute, M.A., Hayes, M.J., Janecke, S.U., Lundin, E.R., McKittrick, M.A., and Olivares, M.D., 1988, Paleogeographic and paleotectonic setting of Laramide sedimentary basins in the central Rocky Mountain region: Geological Society of America Bulletin, v. 100, p. 1023–1039, https://doi.org/10.1130/0016-7606(1988)100<1023:PAPSOL>2.3.CO;2.

Ducea, M., 2001, The California arc: Thick granitic batholiths, eclogitic residues, lithospheric-scale thrusting, and magmatic flare-ups: GSA Today, v. 11, p. 4–10, https://doi.org/10.1130/1052-5173(2001)011<0004:TCATGB>2.0.CO;2.

Ducea, M.N., and Barton, M.D., 2007, Igniting flare-up events in Cordilleran arcs: Geology, v. 35, p. 1047–1050, https://doi.org/10.1130/G23898A.1.

Ducea, M., and Saleeby, J., 1998, A case for delamination of the deep batholithic crust beneath the Sierra Nevada, California: International Geology Review, v. 40, p. 78–93, https://doi.org/10.1080/00206819809465199.

Ducea, M.N., Kidder, S., Chesley, J.T., and Saleeby, J.B., 2009, Tectonic underplating of trench sediments beneath magmatic arcs: The central California example: International Geology Review, v. 51, p. 1–26, https://doi.org/10.1080/00206810802602767.

Ducea, M.N., Saleeby, J.B., and Bergantz, G., 2015, The architecture, chemistry, and evolution of continental magmatic arcs: Annual Review of Earth and Planetary Sciences, v. 43, p. 299–331, https://doi.org/10.1146/annurev-earth-060614-105049.

Dunne, G.C., and Walker, J.D., 2004, Structure and evolution of the East Sierran thrust system, east central California: Tectonics, v. 23, no. 4, https://doi.org/10.1029/2002TC001478.

Eiler, J.M., 2001, Oxygen isotope variations of basaltic lavas and upper mantle rocks: Reviews in Mineralogy and Geochemistry, v. 43, p. 319–364.

Farmer, G.L., and DePaolo, D.J., 1984, Origin of Mesozoic and Tertiary granite in the western United States and implications for Pre-Mesozoic crustal structure: 2. Nd and Sr isotopic studies of unmineralized and Cu- and Mo-mineralized granite in the Precambrian Craton: Journal of Geophysical Research. Solid Earth, v. 89, p. 10141–10160, https://doi.org/10.1029/JB089iB12p10141.

Farmer, G.L., Perry, F.V., Semken, S., Crowe, B., Curtis, D., and DePaolo, D.J., 1989, Isotopic evidence on the structure and origin of subcontinental lithospheric mantle in southern Nevada: Journal of Geophysical Research. Solid Earth, v. 94, p. 7885–7898, https://doi.org/10.1029/JB094iB06p07885.

Farmer, G.L., Glazner, A.F., Wilshire, H.G., Wooden, J.L., Pickthorn, W.J., and Katz, M., 1995, Origin of late Cenozoic basalts at the Cima volcanic field, Mojave Desert, California: Journal of Geophysical Research. Solid Earth, v. 100, p. 8399–8415, https://doi.org/10.1029/95JB00070.

Farmer, G.L., Bailley, T., and Elkins-Tanton, L.T., 2008, Mantle source volumes and the origin of the mid-Tertiary ignimbrite flare-up in the southern Rocky Mountains, western U.S: Lithos, v. 102, p. 279–294, https://doi.org/10.1016/j.lithos.2007.08.014.

Fitz-Díaz, E., Lawton, T.F., Juárez-Arriaga, E., and Chávez-Cabello, G., 2017, The Cretaceous-Paleogene Mexican orogen: Structure, basin development, magmatism and tectonics: Earth-Science Reviews, https://doi.org/10.1016/j.earscirev.2017.03.002.

Gehrels, G., and Pecha, M., 2014, Detrital zircon U-Pb geochronology and Hf isotope geochemistry of Paleozoic and Triassic passive margin strata of western North America: Geosphere, v. 10, p. 49–65, https://doi.org/10.1130/GES00889.1.

Gehrels, G.E., Valencia, V.A., and Ruiz, J., 2008, Enhanced precision, accuracy, efficiency, and spatial resolution of U-Pb ages by laser ablation–multicollector–inductively coupled plasma–mass spectrometry: Geochemistry Geophysics Geosystems, v. 9, https://doi.org/10.1029/2007GC001805.

Glazner, A.F., and O'Neil, J.R., 1989, Crustal structure of the Mojave Desert, California: Inferences from Sr and O Isotope studies of Miocene volcanic rocks: Journal of Geophysical Research, v. 94, p. 7861–7870, https://doi.org/10.1029/JB094iB06p07861.

Glazner, A.F., Farmer, G.L., Hughes, W.T., Wooden, J., and Pickthorn, W., 1991, Contamination of basaltic magma by mafic crust at Amboy and Pisgah Craters, Mojave Desert, California: Journal of Geophysical Research. Solid Earth, v. 96, p. 13673–13691, https://doi.org/10.1029/91JB00175.

Grove, M., Jacobson, C.E., Barth, A.P., and Vucic, A., 2003, Temporal and spatial trends of Late Cretaceous–early Tertiary underplating of Pelona and related schist beneath southern California and southwestern Arizona, *in* Johnson, S.E., Paterson, S.R., Fletcher, J.M., Girty, G.H., Kimbrough, D.L., and Martín-Barajas, A., eds., Tectonic evolution of northwestern Mexico and Southwestern USA: Geological Society of America Special Paper 374, p. 381–406, https://doi.org/10.1130/0-8137-2374-4.381.

Haschke, M., Siebel, W., Günther, A., and Scheuber, E., 2002, Repeated crustal thickening and recycling during the Andean orogeny in north Chile (21°–26°S): Journal of Geophysical Research. Solid Earth, v. 107, https://doi.org/10.1029/2001JB000328.

Hildreth, W., and Moorbath, S., 1988, Crustal contributions to arc magmatism in the Andes of central Chile: Contributions to Mineralogy and Petrology, v. 98, no. 4, p. 455–489, https://doi.org/10.1007/BF00372365.

Humphreys, E.D., 1995, Post-Laramide removal of the Farallon slab, western United States: Geology, v. 23, p. 987–990, https://doi.org/10.1130/0091-7613(1995)023<0987:PLROTF>2.3.CO;2.

Kemp, A.I.S., Hawkesworth, C.J., Collins, W.J., Gray, C.M., and Blevin, P.L., 2009, Isotopic evidence for rapid continental growth in an extensional accretionary orogen: The Tasmanides, eastern Australia: Earth and Planetary Science Letters, v. 284, p. 455–466, https://doi.org/10.1016/j.epsl.2009.05.011.

King, E.M., Valley, J.W., Stockli, D.F., and Wright, J.E., 2004, Oxygen isotope trends of granitic magmatism in the Great Basin: Location of the Precambrian craton boundary as reflected in zircons: Geological Society of America Bulletin, v. 116, p. 451–462, https://doi.org/10.1130/B25324.1.

Kinny, P.D., and Maas, R., 2003, Lu–Hf and Sm–Nd isotope systems in zircon, *in* Hanchar, J.M., and Hoskin, P.W.O., eds., Zircon: Reviews in Mineralogy and Geochemistry, v. 53, p. 327–341, https://doi.org/10.2113/0530327.

Kistler, R.W., 1990, Two different lithosphere types in the Sierra Nevada, California, *in* Anderson J.L., ed., The Nature and Origin of Cordilleran Magmatism: Geological Society of America Memoir 174, p. 271–282, https://doi.org/10.1130/MEM174-p271.

Kistler, R.W., and Peterman, Z.E., 1973, Variations in Sr, Rb, K, Na, and initial Sr^{87}/Sr^{86} in Mesozoic granitic rocks and intruded wall rocks in central California: Geological Society of America Bulletin, v. 84, p. 3489–3512, https://doi.org/10.1130/0016-7606(1973)84<3489:VISRKN>2.0.CO;2.

Kistler, R.W., Wooden, J.L., and Morton, D.M., 2003, Isotopes and ages in the northern Peninsular Ranges batholith, southern California: U.S. Geological Survey Open File Report 2003-489, 45 p.

Kita, N.T., Ushikubo, T., Fu, B., and Valley, J.W., 2009, High precision SIMS oxygen isotope analysis and the effect of sample topography: Chemical Geology, v. 264, p. 43–57, https://doi.org/10.1016/j.chemgeo.2009.02.012.

Lackey, J.S., Valley, J.W., and Saleeby, J.B., 2005, Supracrustal input to magmas in the deep crust of Sierra Nevada batholith: Evidence from high-$\delta^{18}O$ zircon: Earth and Planetary Science Letters, v. 235, p. 315–330, https://doi.org/10.1016/j.epsl.2005.04.003.

Lackey, J.S., Valley, J.W., Chen, J.H., and Stockli, D.F., 2008, Dynamic magma systems, crustal recycling, and alteration in the central Sierra Nevada batholith: The oxygen isotope record: Journal of Petrology, v. 49, p. 1397–1426, https://doi.org/10.1093/petrology/egn030.

Lang, J.R., and Titley, S.R., 1998, Isotopic and geochemical characteristics of Laramide magmatic systems in Arizona and implications for the genesis of porphyry copper deposits: Economic Geology, v. 93, p. 138–170, https://doi.org/10.2113/gsecongeo.93.2.138.

Lawton, T.F., and McMillan, N.J., 1999, Arc abandonment as a cause for passive continental rifting: Comparison of the Jurassic Mexican Borderland rift and the Cenozoic Rio Grande rift: Geology, v. 27, p. 779–782, https://doi.org/10.1130/0091-7613(1999)027<0779:AAAACF>2.3.CO;2.

Leveille, R.A., and Stegen, R.J., 2012, The southwestern North America porphyry copper province, *in* Hedenquist J.W., Harris, M., and Camus, F., eds., Geology and Genesis of Major Copper Deposits and Districts of the World: A Tribute to Richard H. Sillitoe: Society of Economic Geologists, Special Publication 16, p. 361–401.

Lipman, P.W., 1992, Magmatism in the Cordilleran United States; Progress and problems, *in* Burchfiel, B.C., Lipman, P.W., and Zoback, M.L., eds., The Cordilleran Orogen: Conterminous U.S.: Boulder, Colorado, Geological Society of America, Geology of North America, p. 481–514, https://doi.org/10.1130/DNAG-GNA-G3.481.

Liu, L., Gurnis, M., Seton, M., Saleeby, J., Müller, R.D., and Jackson, J.M., 2010, The role of oceanic plateau subduction in the Laramide orogeny: Nature Geoscience, v. 3, p. 353, https://doi.org/10.1038/ngeo829.

Martin, M.W., and Walker, J.D., 1992, Extending the western North American Proterozoic and Paleozoic continental crust through the Mojave Desert: Geology, v. 20, p. 753–756, https://doi.org/10.1130/0091-7613(1992)020<0753:ETWNAP>2.3.CO;2.

Martini, M., Solari, L., and López-Martínez, M., 2014, Correlating the Arperos Basin from Guanajuato, central Mexico, to Santo Tomás, southern Mexico: Implications for the paleogeography and origin of the Guerrero terrane: Geosphere, v. 10, p. 1385–1401, https://doi.org/10.1130/GES01055.1.

McMillan, N.J., 2004, Magmatic record of Laramide subduction and the transition to Tertiary extension: Upper Cretaceous through Eocene igneous rocks of New Mexico, *in* Mack G.H., and Giles, K.A., eds., The Geology of New Mexico: A Geologic History: New Mexico Geological Society Special Publication 11, p. 249–267.

McMillan, N.J., Dickin, A.P., and Haag, D., 2000, Evolution of magma source regions in the Rio Grande rift, southern New Mexico: Geological Society of America Bulletin, v. 112, p. 1582–1593, https://doi.org/10.1130/0016-7606(2000)112<1582:EOMSRI>2.0.CO;2.

McQuarrie, N., and Wernicke, B.P., 2005, An animated tectonic reconstruction of southwestern North America since 36 Ma: Geosphere, v. 1, p. 147–172, https://doi.org/10.1130/GES00016.1.

Miller, C.F., and Barton, M.D., 1990, Phanerozoic plutonism in the Cordilleran interior, USA, *in* Kay S.M., and Rapela, C.W., eds., Plutonism from Antarctica to Alaska: Geological Society of America Special Paper 241, p. 213–231, https://doi.org/10.1130/SPE241-p213.

Miller, J.S., and Glazner, A.F., 1995, Jurassic plutonism and crustal evolution in the central Mojave Desert, California: Contributions to Mineralogy and Petrology, v. 118, p. 379–395, https://doi.org/10.1007/s004100050021.

Miller, J.S., Glazner, A.F., Walker, J.D., and Martin, M.W., 1995, Geochronologic and isotopic evidence for Triassic-Jurassic emplacement of the eugeoclinal allochthon in the Mojave Desert region, California: Geological Society of America Bulletin, v. 107, p. 1441–1457, https://doi.org/10.1130/0016-7606(1995)107<1441:GAIEFT>2.3.CO;2.

Miller, J.S., Glazner, A.F., Farmer, G.L., Suayah, I.B., and Keith, L.A., 2000, A Sr, Nd, and Pb isotopic study of mantle domains and crustal structure from Miocene volcanic rocks in the Mojave Desert, California: Geological Society of America Bulletin, v. 112, p. 1264–1279, https://doi.org/10.1130/0016-7606(2000)112<1264:ASNAPI>2.0.CO;2.

Rämö, T.O., Calzia, J.P., and Kosunen, P.J., 2002, Geochemistry of Mesozoic plutons, southern Death Valley region, California: Insights into the origin of Cordilleran interior magmatism: Contributions to Mineralogy and Petrology, v. 143, p. 416–437, https://doi.org/10.1007/s00410-002-0354-9.

Ramos, V.A., 2009, Anatomy and global context of the Andes: Main geologic features and the Andean orogenic cycle, *in* Kay, S.M., Ramos, V.A., and Dickinson, W.R., eds., Backbone of the Americas: Shallow Subduction, Plateau Uplift, and Ridge and Terrane Collision: Geological Society of America Memoir 204, p. 31–65, https://doi.org/10.1130/2009.1204(02).

Ricketts, J.W., Kelley, S.A., Karlstrom, K.E., Schmandt, B., Donahue, M.S., and van Wijk, J., 2016, Synchronous opening of the Rio Grande rift along its entire length at 25–10 Ma supported by apatite (U-Th)/He and fission-track thermochronology, and evaluation of possible driving mechanisms: Geological Society of America Bulletin, v. 128, p. 397–424, https://doi.org/10.1130/B31223.1.

Riggs, N.R., Reynolds, S.J., Lindner, P.J., Howell, E.R., Barth, A.P., Parker, W.G., and Walker, J.D., 2013, The Early Mesozoic Cordilleran arc and Late Triassic paleotopography: The detrital record in Upper Triassic sedimentary successions on and off the Colorado Plateau: Geosphere, v. 9, p. 602–613, https://doi.org/10.1130/GES00860.1.

Saleeby, J., 2003, Segmentation of the Laramide slab—Evidence from the southern Sierra Nevada region: Geological Society of America Bulletin, v. 115, p. 655–668, https://doi.org/10.1130/0016-7606(2003)115<0655:SOTLSF>2.0.CO;2.

Speed, R.C., and Sleep, N.H., 1982, Antler orogeny and foreland basin: A model: Geological Society of America Bulletin, v. 93, p. 815–828, https://doi.org/10.1130/0016-7606(1982)93<815:AOAFBA>2.0.CO;2.

Spencer, J.E., and Reynolds, S.J., 1990, Relationship between Mesozoic and Cenozoic tectonic features in west central Arizona and adjacent southeastern California: Journal of Geophysical Research. Solid Earth, v. 95, p. 539–555, https://doi.org/10.1029/JB095iB01p00539.

Spencer, J.E., Richard, S.M., Reynolds, S.J., Miller, R.J., Shafiqullah, M., Gilbert, W.G., and Grubensky, M.J., 1995, Spatial and temporal relationships between mid-Tertiary magmatism and extension in southwestern Arizona: Journal of Geophysical Research. Solid Earth, v. 100, p. 10321–10351, https://doi.org/10.1029/94JB02817.

Spencer, J.E., Richard, S.M., Gehrels, G.E., Gleason, J.D., and Dickinson, W.R., 2011, Age and tectonic setting of the Mesozoic McCoy Mountains Formation in western Arizona, USA: Geological Society of America Bulletin, v. 123, p. 1258–1274, https://doi.org/10.1130/B30206.1.

Stewart, J.H., 2005, Evidence for Mojave-Sonora megashear—Systematic left-lateral offset of Neoproterozoic to Lower Jurassic strata and facies, western United States and northwestern Mexico, *in* Anderson, T.H., Nourse, J.A., McKee, J.W., Steiner, M.B., eds., The Mojave-Sonora Megashear Hypothesis: Development, Assessment, and Alternatives: Geological Society of America Special Paper 393, p. 209–231, https://doi.org/10.1130/0-8137-2393-0.209.

Trail, D., Bindeman, I.N., Watson, E.B., and Schmitt, A.K., 2009, Experimental calibration of oxygen isotope fractionation between quartz and zircon: Geochimica et Cosmochimica Acta, v. 73, p. 7110–7126, https://doi.org/10.1016/j.gca.2009.08.024.

Valley, J.W., 2003, Oxygen isotopes in zircon, *in* Hanchar, J.M., and Hoskin, P.W.O., eds., Zircon: Reviews in Mineralogy and Geochemistry, v. 53, p. 343–385.

Valley, J.W., and Kita, N.T., 2009, In situ oxygen isotope geochemistry by ion microprobe, *in* Fayek, M., ed., Secondary ion mass spectrometry in the Earth sciences: Mineralogical Association of Canada Short Course, v. 41, p. 19–63.

Valley, J.W., Bindeman, I.N., and Peck, W.H., 2003, Empirical calibration of oxygen isotope fractionation in zircon: Geochimica et Cosmochimica Acta, v. 67, p. 3257–3266, https://doi.org/10.1016/S0016-7037(03)00090-5.

Vervoort, J.D., Patchett, P.J., Blichert-Toft, J., and Albarède, F., 1999, Relationships between Lu–Hf and Sm–Nd isotopic systems in the global sedimentary system: Earth and Planetary Science Letters, v. 168, p. 79–99, https://doi.org/10.1016/S0012-821X(99)00047-3.

Walker, J.D., 1988, Permian and Triassic rocks of the Mojave Desert and their implications for timing and mechanisms of continental truncation: Tectonics, v. 7, no. 3, p. 685–709, https://doi.org/10.1029/TC007i003p00685.

Wang, X.-L., Coble, M.A., Valley, J.W., Shu, X.-J., Kitajima, K., Spicuzza, M.J., and Sun, T., 2014, Influence of radiation damage on late Jurassic zircon from southern China: Evidence from in situ measurement of oxygen isotopes, laser Raman, U-Pb ages, and trace elements: Chemical Geology, v. 389, p. 122–136, https://doi.org/10.1016/j.chemgeo.2014.09.013.

Wang, K., Plank, T., Walker, J.D., and Smith, E.I., 2002, A mantle melting profile across the Basin and Range, SW USA: Journal of Geophysical Research. Solid Earth, v. 107, https://doi.org/10.1029/2001JB000209.

Wells, M.L., Hoisch, T.D., Cruz-Uribe, A.M., and Vervoort, J.D., 2012, Geodynamics of synconvergent extension and tectonic mode switching: Constraints from the Sevier-Laramide orogen: Tectonics, v. 31, https://doi.org/10.1029/2011TC002913.

Whitmeyer, S.J., and Karlstrom, K.E., 2007, Tectonic model for the Proterozoic growth of North America: Geosphere, v. 3, p. 220–259, https://doi.org/10.1130/GES00055.1.

Wooden, J.L., Barth, A.P., and Mueller, P.A., 2013, Crustal growth and tectonic evolution of the Mojave crustal province: Insights from hafnium isotope systematics in zircons: Lithosphere, v. 5, p. 17–28, https://doi.org/10.1130/L218.1.

Zhu, D.C., Zhao, Z.D., Niu, Y., Mo, X.X., Chung, S.L., Hou, Z.Q., Wang, L.Q., and Wu, F.Y., 2011, The Lhasa Terrane: Record of a microcontinent and its histories of drift and growth: Earth and Planetary Science Letters, v. 301, p. 241–255, https://doi.org/10.1016/j.epsl.2010.11.005.

Science Editor: Aaron J. Cavosie
Associate Editor: Chris Kirkland

Manuscript Received 2 October 2017
Revised Manuscript Received 31 January 2018
Manuscript Accepted 21 May 2018

Printed in the USA